PROCEEDINGS, 49th Workshop on Geothermal Reservoir Engineering
Stanford University, Stanford, California, February 12-14, 2024
SGP-TR-227

Stepwise Development of a Geothermal Reservoir with Shallow Vapor-Dominated and Deep Liquid-Dominated Zones: A Hypothetical Development Scenario of Mataloko Geothermal Field, Indonesia

Vincentius Adven Brilian[1*], Saeful Ghofar Zamianie Putra[2], Alfu Afkar Anniffari[3], Sarah Rania Jasmine[4]

[1]PT Geoenergi Solusi Indonesia ("Geoenergis"), South Jakarta, Indonesia
[2]PT Pertamina Hulu Rokan, Prabumulih, South Sumatra, Indonesia
[3]Department of Geological Engineering, Faculty of Engineering, Gadjah Mada University, Yogyakarta, Indonesia
[4]Schlumberger, Jakarta, Indonesia

*Corresponding author: adven.brilian01@gmail.com

Keywords: stepwise development, geothermal reservoir, liquid-dominated, Mataloko, vapor-dominated

ABSTRACT

Mataloko geothermal field is located in Eastern Nusa Tenggara, Indonesia. Its geothermal reservoir is distinguishable into two main zones: 1) shallow vapor-dominated; and 2) deep liquid-dominated. Unlike in many geothermal reservoirs where a liquid-dominated reservoir underlies a steam cap, the shallow vapor-dominated zone in Mataloko is unique due to its presence within the low permeability cap rock region. Geoscience and well data interpretation suggests that the highly permeable Wae Luja fault provides the permeability for the geothermal fluid from the deep liquid-dominated zone to flow upwards through the cap rock thus forming a shallow steam pocket. In 2000-2006, four exploration wells and two development wells were drilled in the field. Despite all six wells just penetrating the shallow vapor-dominated zone, a 2.5 MWe single-flash geothermal power plant was commissioned in 2010 to utilize the discharge steam. However, the power plant has not been producing since 2015 due to rapid decline of the production from the shallow vapor-dominated zone. This study analyzes the technical and economic feasibility of a hypothetical Mataloko field development scenario by developing both reservoir zones in-stages, assuming that no power plant has been installed yet in the field. This aims to demonstrate an example of a geothermal reservoir development involving a unique vapor-dominated and liquid-dominated zones distinction as it is in Mataloko. In this hypothetical scenario, a development capacity of 22 MWe is proposed by considering the results of resource assessment using the volumetric method for each reservoir zone. The development consists of 2 MWe development of the shallow vapor-dominated zone and 20 MWe development of the deep liquid-dominated zone using two scenarios: Scenario 1 (2+20 MWe) and Scenario 2 (2+10+10 MWe). The 2 MWe power generation from the shallow vapor-dominated zone will be supported by the existing wells. Therefore, the subsequent development drilling will target the deep liquid-dominated reservoir. To support the 20 MWe production from the deep liquid-dominated reservoir, six deep production wells and three deep reinjection wells are required to be drilled. Furthermore, based on the economic analysis, Scenario 2 is more feasible, requiring 102.9 million USD capital expenditure and yielding a project internal rate of return (IRR) of 19%, a project net present value (NPV) of 18.6 million USD, and a payback period of 6 years.

1. INTRODUCTION

Eastern Nusa Tenggara (NTT) is the province with the lowest electrification ratio in Indonesia, as much as 88% in 2020 (Indonesian Directorate General of Electricity, 2021). Moreover, (Indonesian National Electricity Company, 2021) projected the province's electricity demand to grow by 8,8% per year from 1277 GWh in 2021 to 2675 GWh in 2030. Besides, NTT has 1,222.5 MWe geothermal potential with only 12.5 MWe utilized. Through the program named "Flores Geothermal Island", the government intended to develop geothermal energy to increase electrification ratio in NTT and to replace expensive and high-emission diesel power plants. One of the existing geothermal working areas (WKP) in NTT is Mataloko geothermal field, which is located in Golewa District, Ngada Regency, Eastern Nusa Tenggara, as shown in Figure 1. As a result of initial geoscience survey showing that Mataloko is a geothermally active area, the exploration of Mataloko geothermal field started under a Indonesia-Japan research cooperation in 1998-2002 (Matsuda, et al., 2002).

Recent studies by (Jatmiko, et al., 2021) and (Pradhipta, et al., 2019) suggested that Mataloko has two primary zones in its geothermal reservoir: 1) shallow vapor-dominated and 2) deep liquid-dominated. The shallow vapor-dominated zone in Mataloko is distinct from other geothermal reservoirs since it is located within the low permeability cap rock area, as opposed to many other geothermal reservoirs where a liquid-dominated reservoir underneath a steam cap. Geoscience and well data interpretation shows that the highly permeable Wae Luja fault provides the permeability for the geothermal fluid from the deep liquid-dominated zone to move upwards through the cap rock thereby creating a shallow steam pocket. Two development wells and four exploration wells were drilled in the field between 2000 and 2006 (Fauziyah & Daud, 2019). The discharge steam was used to power a 2.5 MWe single-flash geothermal power plant that was put into service in 2010 despite the fact that all six wells only barely penetrated the shallow vapor-dominated zone. But because of the sharp drop in output from the shallow vapor-dominated zone, the power plant has not been operating since 2015. Assuming that no power plant has yet been constructed in the field, this study examines the technical and financial viability of a hypothetical Mataloko field development scenario that involves developing both reservoir zones incrementally. The purpose of this is to provide an example of a geothermal reservoir development that involves the distinction between vapor-dominated and liquid-dominated zones, as found in Mataloko.

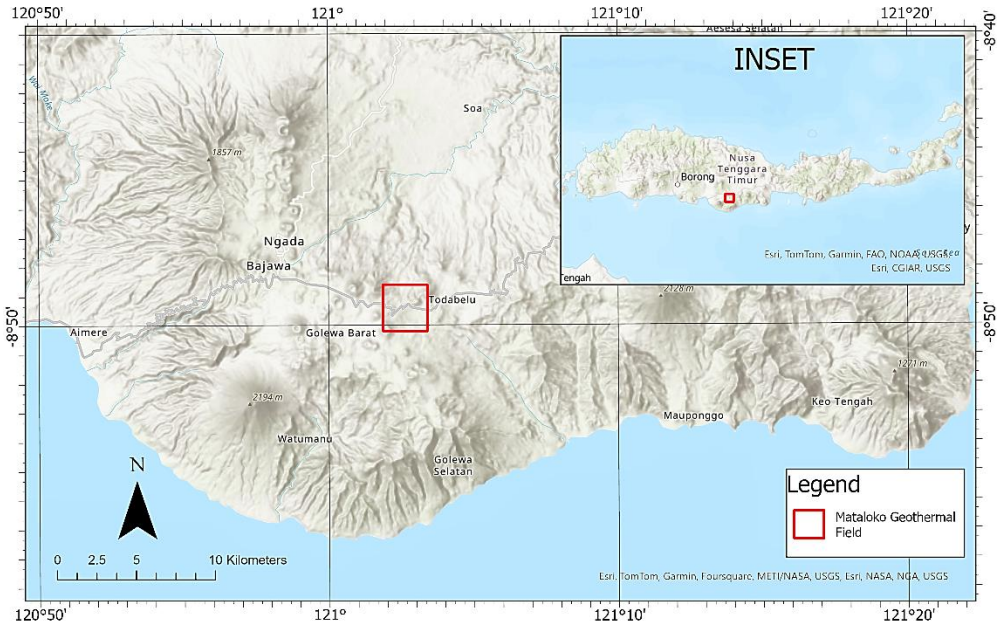

Figure 1: Geographic map of Mataloko Geothermal Field.

2. GEOSCIENCE REVIEW

2.1 Geology

The Mataloko geothermal field is part of the greater Bajawa geothermal area and located on the eastern part of Indonesia, on the island of Flores. The geomorphological features in this location are largely affected by the volcanic activities that have occurred over millions of years. In terms of geomorphology, The Mataloko geothermal field is located on the eastern slope of Bajawa complex forming a large body of caldera, with approximately 10 km in diameter, resulting from large explosive eruption occurring around 1.2 million years ago (Widodo et al., 2002). The field is surrounded by cinder cones showing the same characteristics, including magma affinity, lithology, and eruption type, implying the same source of magma chamber. The elevation ranges from 1.000 – 1.900 masl (Ramdhan, 2019). Lithology is dominated by the products of volcanic activities, such as tuff, lava, andesite, and breccia. Meanwhile, the geological structure is controlled by regional tectonism, driven by subduction activities.

2.1.1 Geological Structure

Structure plays an important role in geothermal activities that will drive the geothermal system. This aspect of geothermal could increase the secondary permeability and play as the upflow pathway of the fluid. Regional fault systems in the surrounding area of Mataloko geothermal field are driven by subduction process that produced SE-NW fault trend. Figure 2 shows the map of geomorphological and geological structure in Mataloko geothermal field. The major faults aligned with the trend are Boba Normal Fault, Hubasora Normal Fault, and Laja Normal Fault. However, several fault systems, such as Matawae 1 Dextral Fault, Triwulina Sinistral Fault, Wae Luja Normal Fault, and Taranage Sinistral Fault, are resulted from later tectonism creating new trend spreading in SW-NE direction. This new trend is believed as important role in the creation of geothermal system in Mataloko. Moreover, recent study shows that Wae Luja Fault is responsible for the upflow pathway in geothermal fluid circulation since it has good permeability compared to the other faults, as it is shown by the geothermal manifestations, for instance fumarole and hot spring. Eventhough faults role as secondary permeable, the other faults are considered as the impermeable boundary in the system (Jatmiko, et al., 2021).

2.1.2 Lithology

Lithology plays a significant role in geothermal system as it affects the permeability which directly impacts geothermal fluid circulation. Figure 3 shows the geological map and cross section of Mataloko geothermal field. Based on chronological data of volcanic events, the study area is classified as 3 periods of volcanic activities that result in different types of lithology. The oldest rock consists of green tuff and Watumanu lava, which are later considered as the basement rock approximately formed in 2.4 – 2.37 Ma. The second period is marked by old volcanic activites of Rotogesa volcanic (consisting of lava flow, pyroclastic flow, and laharic deposit), Wolo Pena volcanic cone, Wolo Roge, Wolo Sasa, and Wolo Pure volcanic cone, formed in 1.1 – 1.6 Ma. Further volcanic activity, the younger activity, is shown by volcanic cones and Wolo Belu lava dome, spreaded in NW-SE direction, which later is assumed affected by geological structure (Nanlohy, et al., 2002).

Geological and stratigraphic data show that Mataloko area consists of 4 rock units, namely Older volcanic rocks (V1), Bajawa volcanic rocks (Bv), Cinder Cone products (C1, C2), and Aimere tuff (At) & Inerie volcano (Ie). Older volcanic rocks (V1) are composed by pyroxene-andesitic lava, pyroclastic rocks, lahar deposits and olivine-basalt formed 1.1 – 1.6 Ma. Bajawa volcanic rocks (Bv) consists mainly of pyroclastic flow and pyroxene-andesitic lava which unconformably overly Older volcanic rocks. Cinder Cone products (C1, C2) are marked mainly by volcanic products (andesitic lava and scoria/pumice) and volcaniclastic deposits spreading along Bajawa depression. Aimere tuff (At) & Inerie volcano (Ie) consists of tuff and andesitic lava, and other pyroclastic materials (Otake et al., 2002).

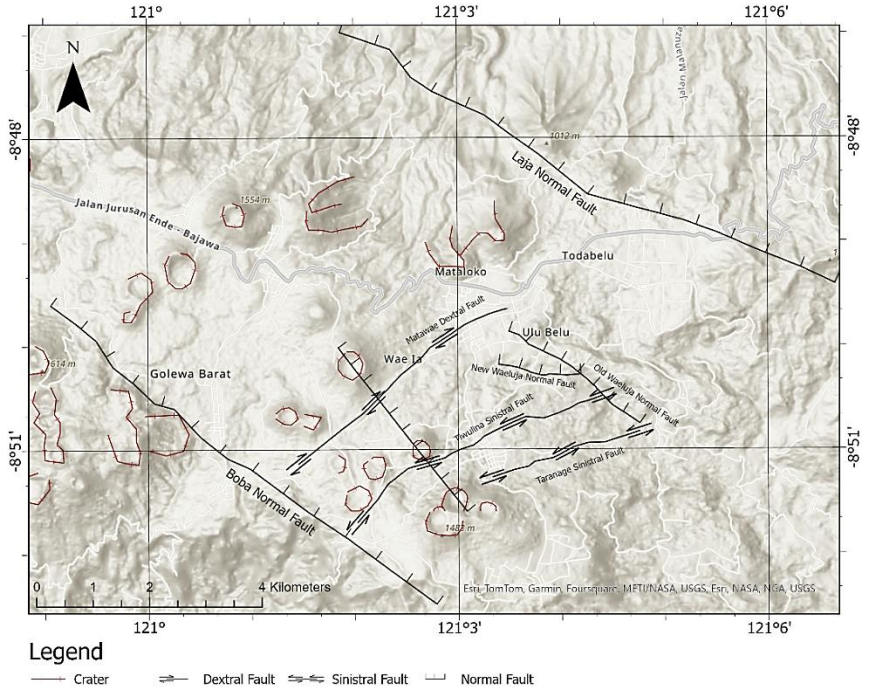

Figure 2: Geomorphological and Geological Structure Map of Mataloko Field (Jatmiko, et al., 2021) (Nanlohy, et al., 2002).

The alteration minerals that can be identified in Mataloko Geothermal Field are alunite, kaolinite, montmorillonite, cristobalite, quartz, pyrophyllite, zeolite, as well as sulphur and sulphide mineral such as pyrite. The alunite zone is interpreted as the upflow zone in this geothermal system (Nahlony et al., 2001). Alunite indicates that the mineral is associated with high sulfidation acidic fluid whereas kaolinite, halloysite, and dickite indicates medium/normal pH and low forming temperature.

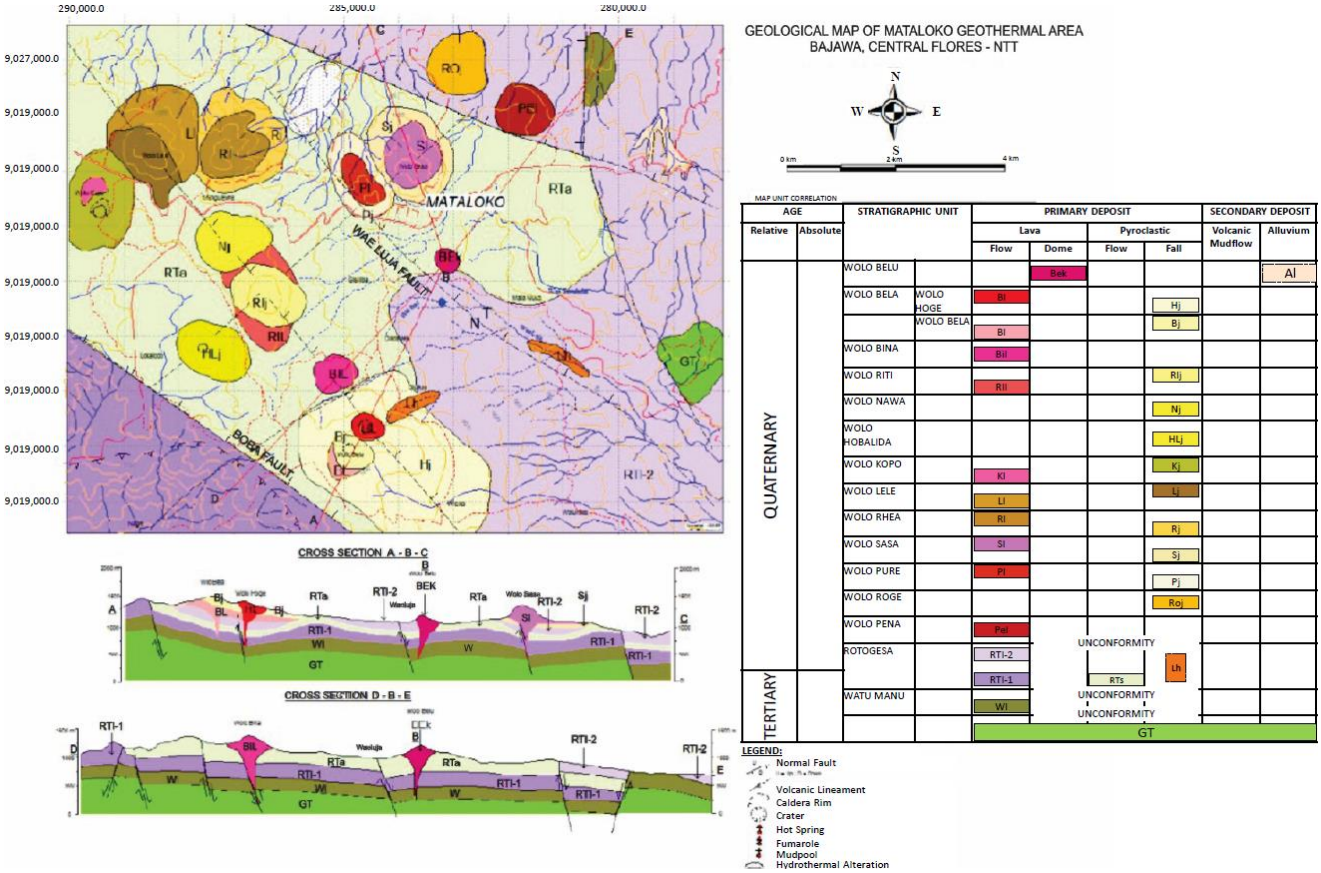

Figure 3: Geological Map and Cross Section of Mataloko Field (Nanlohy, et al., 2002).

2.2 Geophysics

Geophysical studies were carried out to determine the physical and geometrical of the subsurface geothermal system, especially the cap rock or the geological structures. The geophysical studies that have been performed in Mataloko include magnetotelluric (MT), gravity, and magnetic, method.

2.2.1 Magnetotelluric Method

MT is used to image the subsurface resistivity that indicates the presence of clay cap or impermeable cap of a geothermal system. The resistivity could differentiate types of alteration in the subsurface. The resistivity of the propylitic alteration zone generally varies from 10-60 ohm.m. However, clay cap is characterized by low resistivity (1-10 ohm.m) due to the presence of the higher Cation Exchange Capacity clay mineral (Usher, 2000). Based on Figure 4, it can be interpreted that there is a low resistivity zone up to 100 m depth that indicates the clay cap. However, at 0 masl, the resistivity does not show a low resistivity zone but shows a steep high contrast resistivity gradient which might be a hidden fault. Furthermore, the MT data was processed by (Uchida, 2005) to make 3D MT. The result supported the previous interpretation in which based on the resistivity depth slicing in Figure 5, the low resistivity zone in the SW-NE direction starts from 200-1000 m depths that indicates a clay cap zone.

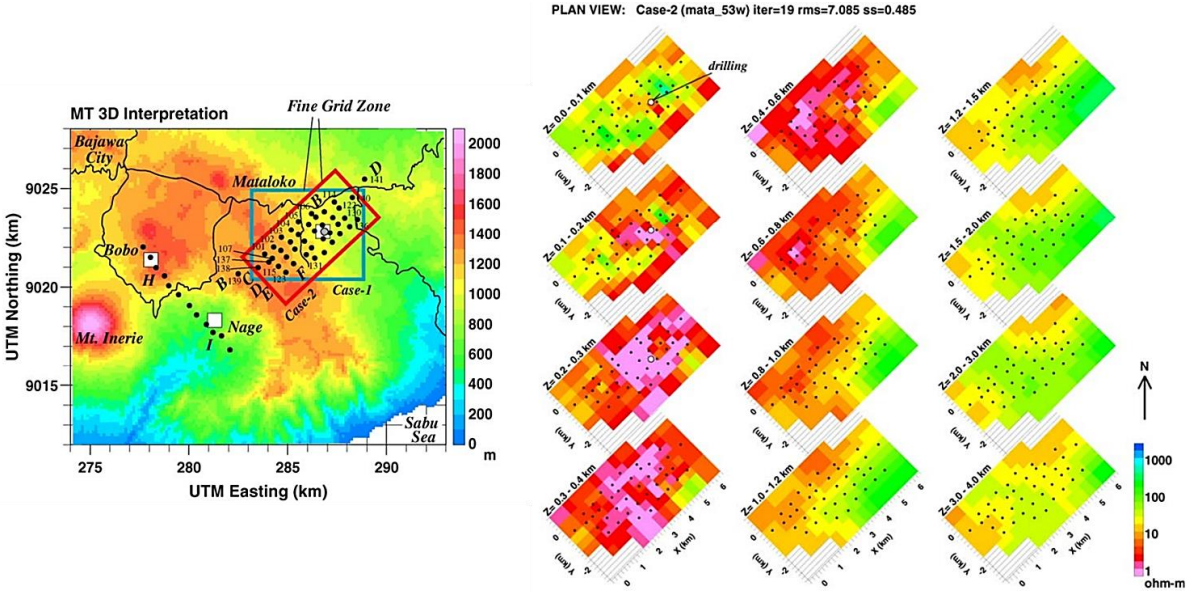

Figure 4: MT Station on Topographic Contour (Left) and Depth-Slice Resistivity Sections of 3D Mataloko MT Model (Right) (Uchida, 2005).

In the surface resistivity, it also shows a low resistivity anomaly that supported by the presence of thermal manifestation. Based on the direct data from two shallow exploration wells of MT-1 and MT-2, kaolinite, montmorillonite, and wairakite in the volcanic rock were present as the major clay alteration mineral. Montmorillonite-rich rocks correspond to a conductive layer, i.e. cap layer of reservoir. Meanwhile, the wairakite found in MT-2 indicates the presence of high temperature geothermal fluid up to 200 m depths. However, based on the interpretation of SW-NE and N-S resistivity cross sections in Figure 5, the clay cap zone starts from the near-surface elevation down to the base of conductive (BOC) at (-100)-200 masl. Therefore, the high temperature geothermal fluid might be circulating upward within the impermeable clay cap through a fracture zone possibly controlled by Wae Luja Fault.

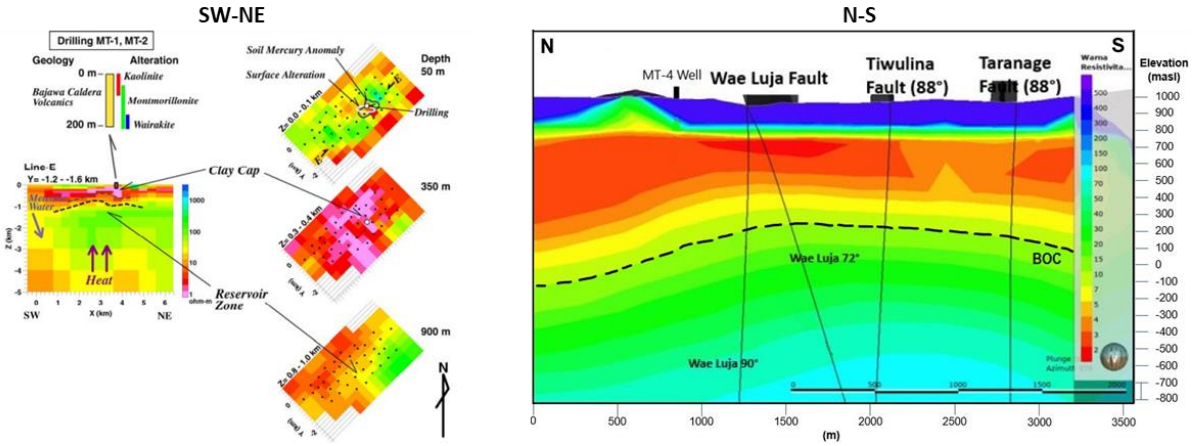

Figure 5: SW-NE (Left) and N-S (Right) Resistivity Cross Sections (Uchida, 2005) (Sumotarto, et al., 2021).

2.2.2. Gravity and Magnetic Method

Gravity method is a method to image the subsurface based on difference of density in each rock or structure. This method is very effective to seek for hidden/burried structures that are invisible from the surface. Gravity data is divided into regional and residual, where residual data show more local structure and density and vice versa. One of the ways to interpret the gravity data is by using second vertical derivative (SVD) method on the residual data to enhance the anomaly. Based on Figure 6, there are four potential structures: 1) NW-SE fault near Naga and Tiworiwa; 2) broad concealed fault in north side of the map near the Bodo Village; 3) contrast impedance in the southeast side of the map; and 4) Wae Luja Fault at Mataloko. The Wae Luja Fault is one of structures that controlled the the field's permeability as the upflow path, which is proved by the presence of Wairekite mineral at the clay cap depths. The other fault potentially become a recharge zone for the Mataloko prospect (Pradhipta, et al., 2019).

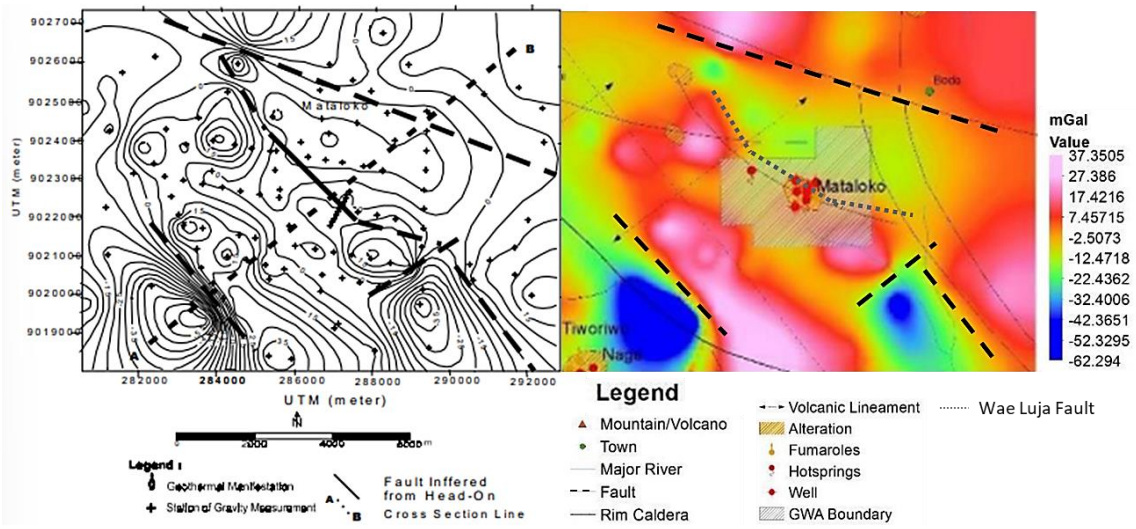

Figure 6: 2nd Order Derivative of Residual Bouguer Anomaly Interpretation. Modified from: (Dwipa, et al., 2001).

Magnetic residual map supports the previous resistivity and gravity data. Firstly, the magnetic response in the centre of Mataloko field shows a negative anomaly (<100 nTesla), which could be affected by the heating process that cause demagnetization of rock due to alteration process. The resistivity response in Figure 7 conforms with magnetic response. Secondly, the magnetic response shows a lineament that is similar to the previous gravity data that indicate the presence of hidden fault in north and south sides of Mataloko field.

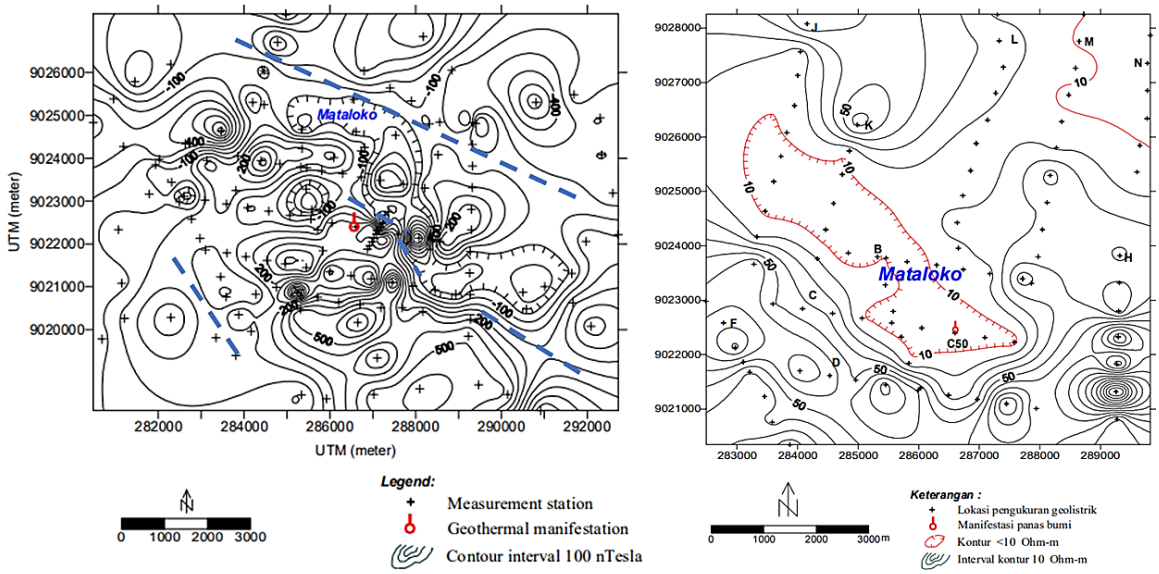

Figure 7: Magnetic Residual Map (Left) from DC Resistivity Method (Right). Modified from: (Dwipa, et al., 2001).

2.3 Geochemistry

Subsurface temperature, origin, and flow direction of fluid in a geothermal system might help locating the reservoir of a geothermal system. Such can be obtained by geochemistry analysis of water or gas from manifestations around WKP Mataloko, shown in Figure 8. In this study, the chemical composition of the analyzed water samples in Mataloko are obtained from previous studies.

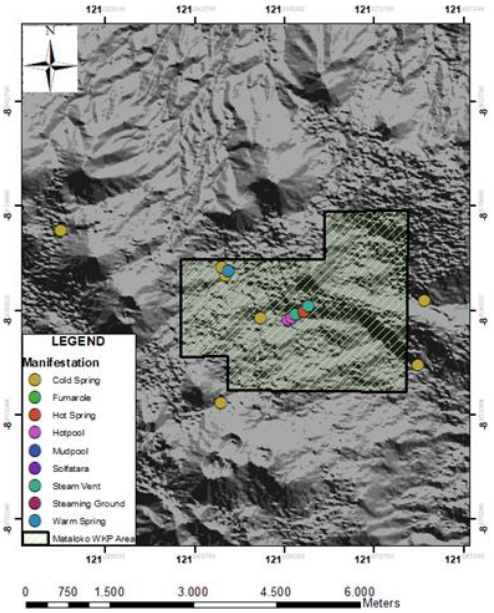

Figure 8: Surface manifestations around WKP Mataloko.

Briefly, the type of surface manifestation are dominated by hot springs, but fumarole is also present. The surface manifestations around Waeluja/Waebeli river has a temperature ranging from 40°-98°C with the pH of approximately 3, and the hot springs have a flow rate less than 0.5 LPM. To determine the fluid type of surface manifestations, this study uses the ternary diagram plot with the parameter of chloride, sulphate, and bicarbonate content from surface manifestation water samples, as shown in Figure 9.

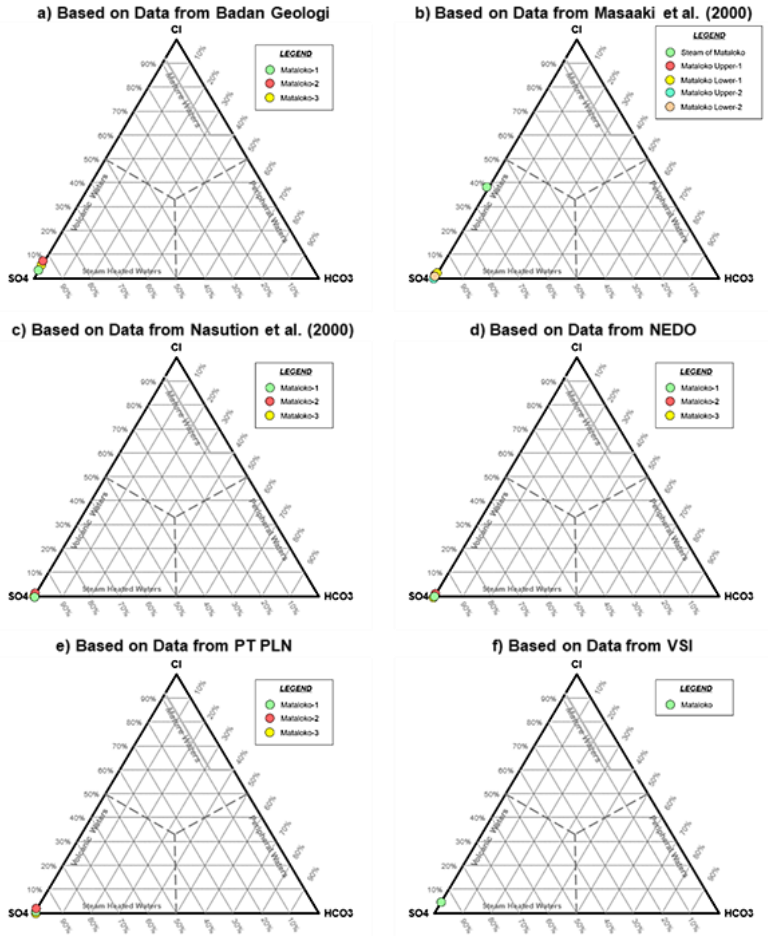

Figure 9: Cl-SO_4-HCO_3 Ternary Diagram of Surface Manifestations.

Most of the fluid samples tested from surface manifestations in Matoloko are high in SO_4 content. Out of 18 existing samples, 17 are interpreted to be sulphate water, while 1 sample is interpreted to be chloride-sulphate water. Sulphate waters are commonly formed because of geothermal gases that condense into groundwater. Meanwhile, chloride-sulphate waters can be formed due to several reasons according to (Nicholson, 1993), which are either because of: 1) mixing of chloride and sulphate water on the way up; 2) near-surface discharge and oxidation of H_2S in chloride waters; 3) near-surface condensation of volcanic gases into meteoric waters; 4) condensation of magmatic vapor at depth, or 5) passage of chloride fluids through sulphate-bearing sequences. Both sulphate waters and chloride-waters are not reliable for interpretation of reservoir temperature because both types of water do not represent the actual reservoir condition and temperature due to a certain process that is done to the reservoir water either it is mixing, condensation, or any other processes while the reservoir water is moving towards the surface. Hence, geothermometer using surface manifestation samples cannot be used to determine the reservoir temperature. In order to justify this, based on the plotted Na-K-Mg Ternary Diagram as shown in Figure 10, all samples of surface manifestation water are considered immature waters, thus water geothermometry is unreliable. Therefore, gas geochemistry of fumarole and exploration well's discharge fluid shall be conducted to estimate the reservoir temperature.

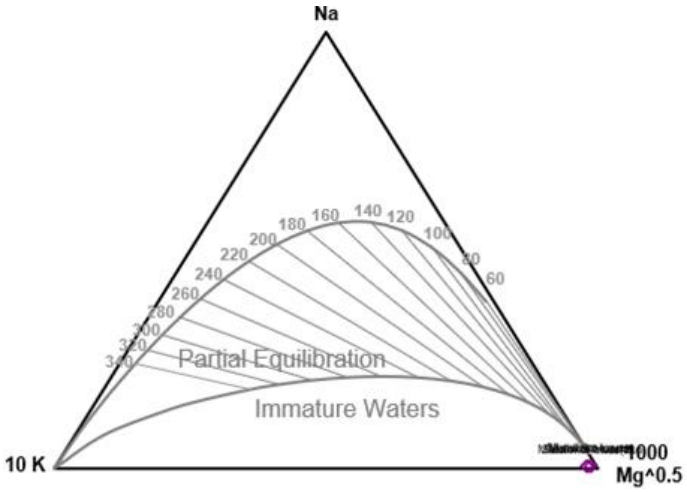

Figure 10: Na-K-Mg Ternary Diagram of Mataloko Surface Manifestations.

3. WELL DATA REVIEW

3.1 General Overview of Existing Wells

The first well drilled in the field was a temperature gradient well (MTL-1). Subsequently, 2 exploration (MT-1 and MT-2), 2 delineation (MT-3 and MT-4), and 2 development (MT-5 and MT-6) were drilled. The well location and general information are shown in Figure 11 and Table 1, respectively. The results of exploration and delineation drilling are reviewed to confirm the resource's existence, temperature, size, permeability, and fluid characteristics based on direct subsurface data. Meanwhile, the results of development drilling are reviewed to extract additional data that improve the understanding of the geothermal system.

Table 1: General Information of the Existing Wells in Mataloko Geothermal Field (Kasbani, et al., 2004).

Parameter	MTL-1	MT-1	MT-2	MT-3	MT-4	MT-5	MT-6
Drilling Data							
Purpose	Temp. grad.	Exploration	Exploration	Delineation	Delineation	Development	Development
Compl. date	1999	2000	2001	2003	2003	2005	2006
Elevation (masl)	939	953	953	962	983	962	n/a
Type	Vertical temp. grad. hole	Vertical slimhole	Vertical slimhole	Vertical standard hole	Vertical standard hole	Vertical standard hole	Vertical standard hole
TVD (m)	103.2	207.3	180	613	756.5	378.2	123.8
TLC zone (mMD)	98.3	-	-	-	700-757	155; 283; 341	-
PLC zone (mMD)	13.2	-	-	-	643	-	-
Feed zone (mMD)	-	207.3	130-180	300-400	250	365	-
Transmissivity (Darcy meter)	-	-	14.43	-	-	69.6	-
Skin factor	-	-	-5.58	-	-	-10.9	-
Discharge fluid	Steam blowout	Steam blowout	Superheated steam	Saturated steam	Two-phase	Saturated steam	-
Current status	Plugged	Plugged	Monitoring	Production	Monitoring	Production	Reinjection

Well Flow Testing and P-T Logging Data							
Steam flow rate (tph)	-	-	17.1	2.89	1.54 – 2.15	20.36; 17.5	-
Wellhead pres. (barg)	-	-	4.5	4.5	5	3; 4.5	-
Enthalpy (kJ/kg)	-	-	2785	2727	-	2739	-
P-T logging depth (m)	-	-	175	540	747	155	-
Maximum downhole temp. (^{o}C)	115	> 200	194	204.08	205.52	103.7	-
Well output (MWe)	-	-	2.07	0.36	-	2.24; 2.12	-
NCG (wt%)	-	-	0.61-0.69	-	-	-	-

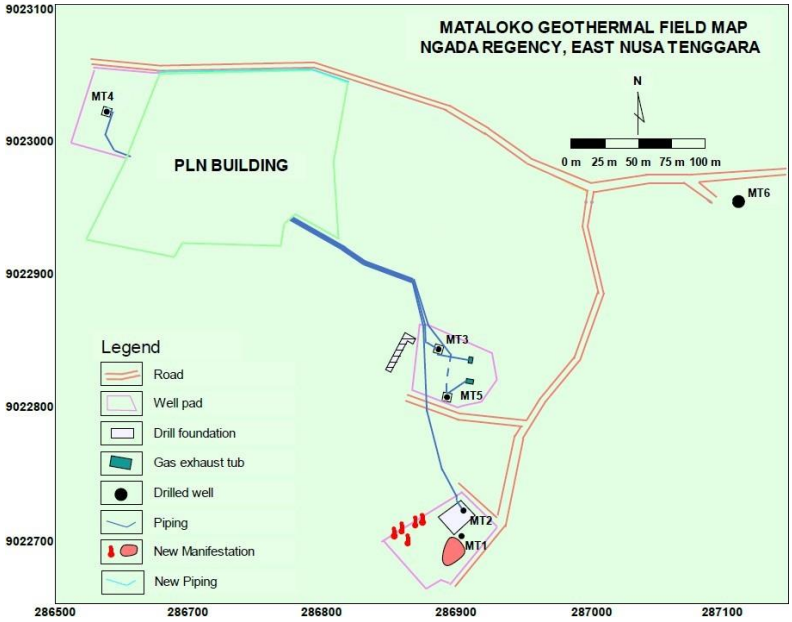

Figure 11: Location Map of the Existing Wells in Mataloko Geothermal Field (Ahmad, et al., 2022).

3.2 MT-1 and MT-2 Exploration Wells

3.2.1 MT-1 and MT-2 Drilling and Well Geology

The drilling of MT-1 started on October 11th, 2000, at an elevation of 953 masl. At the 189-207 m depths (746-764 masl), the rate of penetration was faster than at the shallower depths and the returning mud temperature was higher. These indicate the possibility of the presence of geothermal fluids. The drilling halted at the 207 m depth to install a production casing and blowout preventer (BOP). However, a steam blowout started occuring before the BOP was installed. Before killing the well, grouting was performed to consolidate shallow formations around MT-1 by injecting cement slurry. After the grouting was successful, MT-1 was killed by cement plugging (Sueyoshi, et al., 2002). The experience of drilling MT-1 prompted the use of consolidation grouting prior to drilling MT-2. The drilling of MT-2 started on January 5th, 2001, at an elevation of 953 masl using a vertical standard hole to the depth of 180 m without a blowout. Starting from the 155 m depth, the returning mud temperature started to rise similarly to what occurred when the drilling of MT-1 entered the steam zone (Sueyoshi, et al., 2002).

Both MT-1 and MT-2 were drilled entirely within the Bajawa Caldera Volcanics (Bc) stratigraphic unit. The lithology of MT-2 is very similar to MT-1 that it consists of tuff breccia, ash tuff, andesite, hornblende andesite, and pyroxene. All rock cuttings have been altered into smectite and kaolinite clays, pyrite (with/without carbonate), secondary quartz, anhydrite, illite, and zeolite. Further analysis of rock cuttings undergone through XRD analysis shows several hidrothermal alteration minerals that occurs which are montmorillonite, kaolinite, heulandite, wairakite, quartz, crtistobalite, feldspar, clacite and pyrite with minor chlorite/montmorillonite mixes-layer, sericite-montmorillonite mixed-layer, yugawaralite, epistilbite, alunite, gypsum, anhydrite, goethite, magnetite, and gibbsite. Specifically wairakite indicates the existence of hydrothermal activity on a temperature of 200-300^{o}C. The hydrothermal alteration of MT-2 belongs to argillic type that represents the clay cap with the alteration intensity of medium-to-high (SM/TM = 30-90%) and 15-60% swelling clay. Moreover, static loss of 42 lpm at the 162.4 m depth indicates a very fine fracture zone (Sitorus, et al., 2001).

3.2.2 MT-2 P-T Logging

Five P-T loggings were performed with the results are shown in Figure 12**.** At the 130-175 m depths, the temperature increased from 184°C to 194°C, which corresponds to the feed zone between 130-185 m depths likely controlled by Wae Luja fault's fracture zone (Nanlohy, et al., 2002). Based on the pressure build-up test (PBU) in July 2001, the feed zone has high transmissivity of 14.43 Darcy-meters and skin factor of -5.58, which characterizes a fracture zone. The highest temperature was 194°C at 175 m depth (778 masl).

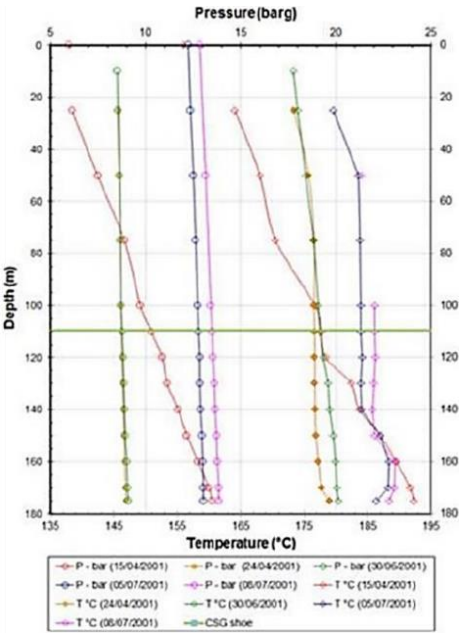

Figure 12: Pressure-Temperature Logs of MT-2 Well (Wahyuningsih & Sitorus, 2004).

3.2.3 MT-2 Well Flow Testing

A short-term flow test using lip pressure method was done at MT-2 in January 2001. The well discharged 16.34 tph of saturated steam at 3.63 barg WHP with the enthalpy of 2713-2727 kJ/kg. At 5.79-5.88 barg WHP, the steam flow rate was 14.5-14.7 tph with the temperature of 135-140°C. Furthermore, a long-term flow test using orifice method was performed between April-July 2001 and the results are shown in Figure 13 (Sitorus, et al., 2002).

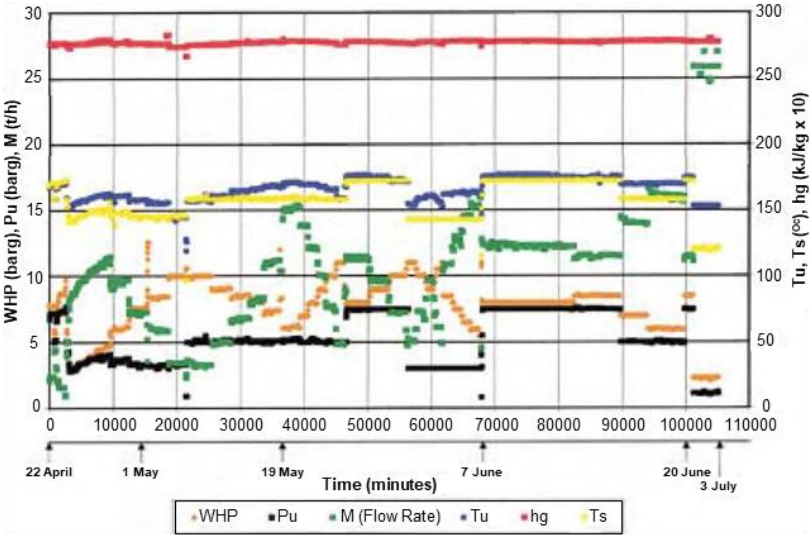

Figure 13: MT-2 Well Long-Term Flow Test Results (Sitorus, et al., 2002).

The long-term flow test data are used to synthesize the deliverability curve of MT-2, as shown in Figure 14. Subsequently, calculation of the optimum operating condition to generate the highest well output was performed by assuming the turbine outlet pressure of 0.15 bara, turbine isentropic efficiency of 80%, and neglecting mass and heat losses. The results in show that MT-2 generates the highest output of 2.07 MWe at 4.5 barg WHP and discharges 17.1 tph of superheated steam with the enthalpy of 2785 kJ/kg. This WHP matches with typical minimum turbine inlet pressure for commercial condensing turbines of 5.5 bara (4.5 barg) (Suhanto & Arsadipura, 2006).

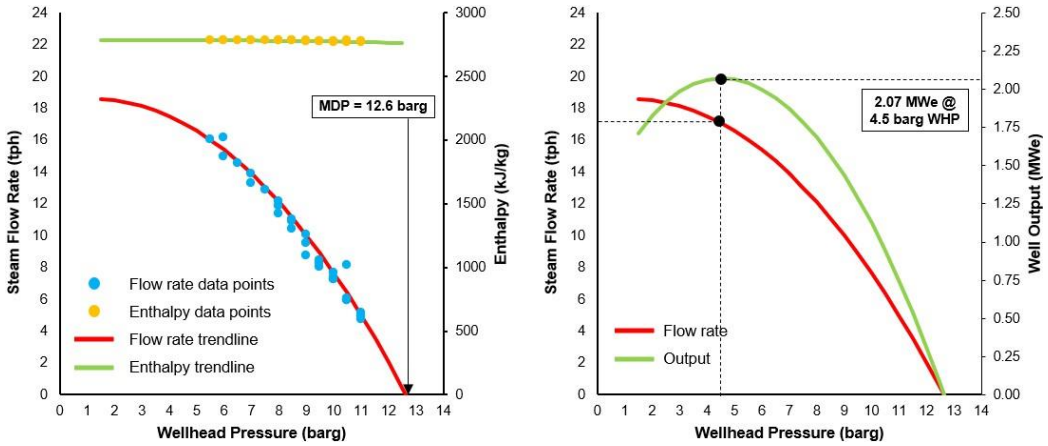

Figure 14: MT-2 Well Flow Rate and Enthalpy vs. WHP (Left); Flow Rate and Power Output vs. WHP (Right).

The discharge steam of MT-2 has a very low non-condensable gas (NCG) content, which is 0.61-0.69 wt%. The NCG content is dominated by CO_2 (91 mole%), while the rest is H_2S and other residual gases. The low NCG content indicates that the steam is likely non-corrosive (Sitorus, et al., 2002). Moreover, low NCG content and a relatively abundant occurence of CO_2, can be interpreted that that well MT-2 discharge steam does not directly come from the heat source, but rather from a liquid-dominated reservoir that exists deeper below the well (Matsuda, et al., 2002). To identify the source of well MT-2 discharge steam, this study conducts stable isotope analysis. Based on the stable isotope data of well MT-2 and Mataloko fumaroles, $\delta^{18}O$ (H_2O) and δD (H_2O) data are plotted into a cross plot diagram as shown in Figure 15 which has a global meteoric water line and local meteoric water line (Matsuda, 2002). MT-2 discharge steams are plotted relatively close with both global and local meteoric water line. However based on the plotting and the local meteoric water line alone, MT-2 discharge steams has a $\delta^{18}O$ positive shift which might suggests that it originates from meteoric water and it most likely happened because of water-rock interaction (Giggenbach & Stewart, 1982).

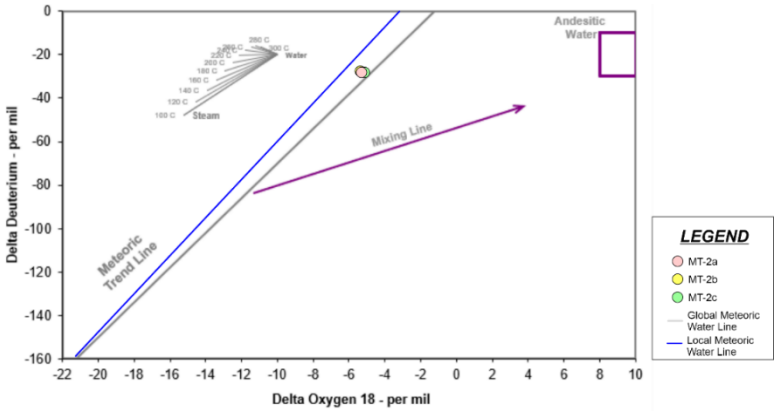

Figure 15: MT-2 Well Steam Discharge Isotope Plot to Determine the Fluid Origin.

Due to the high content of SO_4 in surface manifesations of Mataloko area, gas geochemistry from MT-2 well discharge is used to estimate the reservoir temperature. Hydrogen isotope temperature calculation using different formulas were calculated are listed in Table 2. The lowest calculated temperature from the well discharge is 232°C based on the H_2-CH_4 pair temperature calculation (D'Amore & Panichi, 1987). Supported by the occurence of Wairakite XRD analysis results of MT-2 well cuttings and also the P-T log which records the temperature of 175°C at the shallowest feed zone of MT-2 well, it is indicated that a shallow steam-dominated reservoir exists with a temperature estimated around 175-232°C. Meanwhile, other hydrogen isotope temperature calculations vary surrounding in a nearer range with each other of 270-306°C (THA and TD2 calculation is not accounted due to the calculation results being 30-40°C than the other calculation, interpretated that calculation results are overestimated which is caused by the loss of Ar by vapor loss in the reservoir (Matsuda, et al., 2002). Supported by the low NCG content, it is interpreted that a deeper water-dominated reservoir exists with an estimated temperature of 270-306°C.

Table 2: Hydrogen Isotope Temperature Results Using Different Formulas (Matsuda, et al., 2002).

MT-2 Well Discharge Sample Code	Sampling Date	TDAP (°C)	THA (°C)	TCA (°C)	TFT-HSH (°C)	TDC (°C)	TD1 (°C)	TD2 (°C)
MT-2a	23/01/2001	271	335	293	305	275	232	334
MT-2b	24/01/2001	270	340	296	306	-	-	-
MT-2c	25/01/2001	273	343	298	304	-	-	-

3.3 MT-3 and MT-4 Exploration Wells

3.3.1 MT-3 and MT-4 Drilling and Well Geology

Delination drilling of MT-3 and MT-4 wells were performed in 2003. Both wells used vertical standard hole-type. MT-3 was drilled at an elevation of 962 masl with a total depth of 613 m. Meanwhile, MT-4 was drilled at an elevation of 983 masl with a total depth of 756.5 m. The well geology and casing design of MT-3 and MT-4 are shown in Figure 16. Throughout the drilling of MT-3, no lost circulation (both TLC and PLC) occured. This infers that MT-3 well lithology is characterized by rocks with low permeability (Wahyuningsih & Sitorus, 2004). Up to the 196 m depth, the well lithology is characterized by alternating altered tuff breccia and altered andesite. Furthermore, the lithology at the 196-613 m depths is characterized by altered andesite containing red-brown paleosoil at the 275-500 m depths. All rocks are hydrothermal altered with the alteration intensity of medium-to-high (SM/TM = 20-80%). By considering the hydrothermal alteration types, MT-3 lithology can be categorized into overburden (0-6 m depths or 956-962 masl), argillic zone (6-539 m depths or 423-962 masl) that represents clay cap, and propylitic zone (539-613 m depths or 349-423 masl) that represents reservoir zone (Kasbani, et al., 2004).

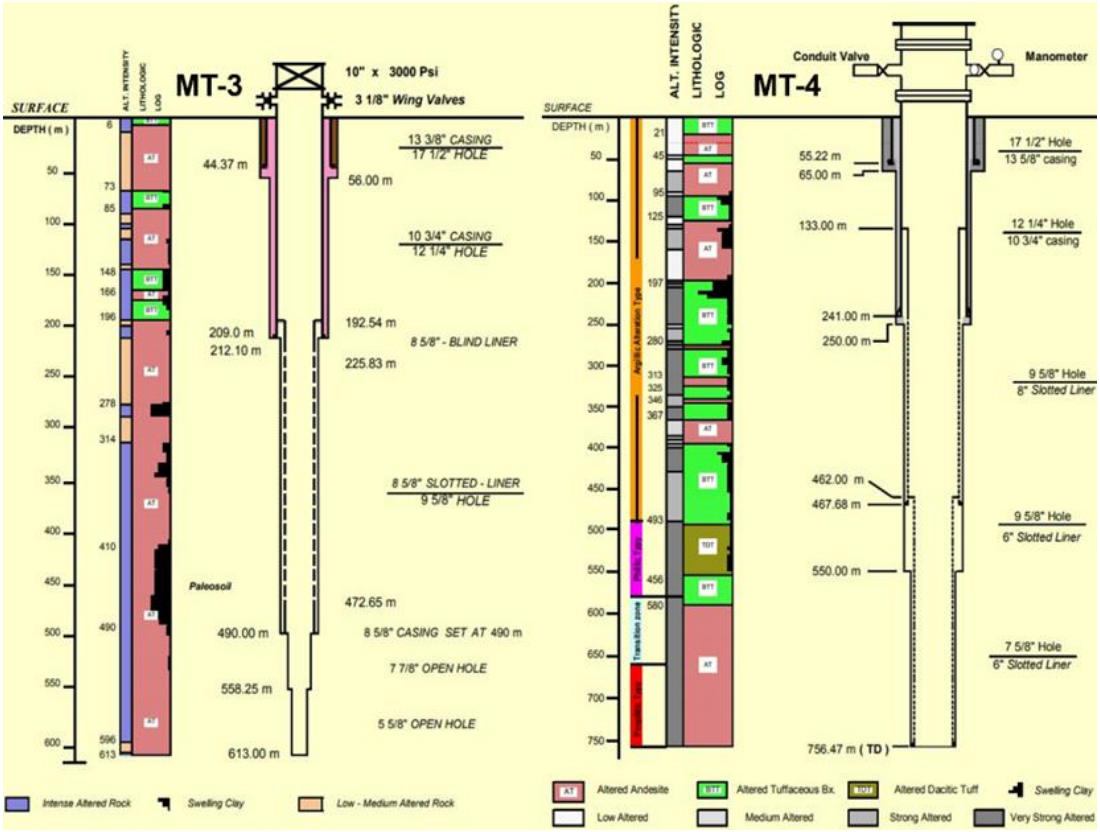

Figure 16: MT-3 and MT-4 Wells Geology and Casing Design (Kasbani, et al., 2004).

Meanwhile, throughout the drilling of MT-4, both PLC and TLC occurred at the depths of 643 m and 700-757 m, respectively. This infers that the MT-4 well lithology is characterized by rocks with medium permeability (Wahyuningsih & Sitorus, 2004). The MT-4 well lithology up to the 756.6 m depth is characterized by alternating altered tuff breccia, altered dacitic tuff, and altered andesite with low-to-high alteration intensity (SM/TM = 10-85%). By considering the hydrothermal alteration types, MT-4 lithology can be categorized into overburden (0-3 m depths or 980-983 masl), argillic zone (3-493 m depths or 490-980 masl) that represents clay cap, phyllic zone (493-556 m depths or 427-490 masl), transition zone (556-659 m depths or 324-427 masl), and propylitic zone (659-756.5 m depths or 226.5-324 masl) that represents reservoir zone (Kasbani, et al., 2004).

3.3.2 MT-3 and MT-4 P-T Logging

One shut-in and three flowing P-T logging were performed at MT-3 well. Compared to the flowing P-T log, the shut-in P-T log representes better the static condition of the reservoir during natural-state since shut-in wells after the drilling eventually achieve pressure and temperature equilibrium with the surrounding formation (Pradhipta et al., 2019). Meanwhile, only one flowing P-T logging was performed at MT-4. The P-T logs of MT-3 and MT-4 are shown in Figure 17. The flowing P-T log of MT-3 at the wellhead pressure (WHP) of 5.5 barg and 6.0 barg shows that the wellbore is filled by a steam column and water column. The top of the steam column under these WHP configurations is at the depths of 350 m (613 masl) and 300 m (662 masl), respectively. The highest recorded wellbore temperature by the flowing P-T log was 204^{o}C at the depth of 541 m (422 masl).

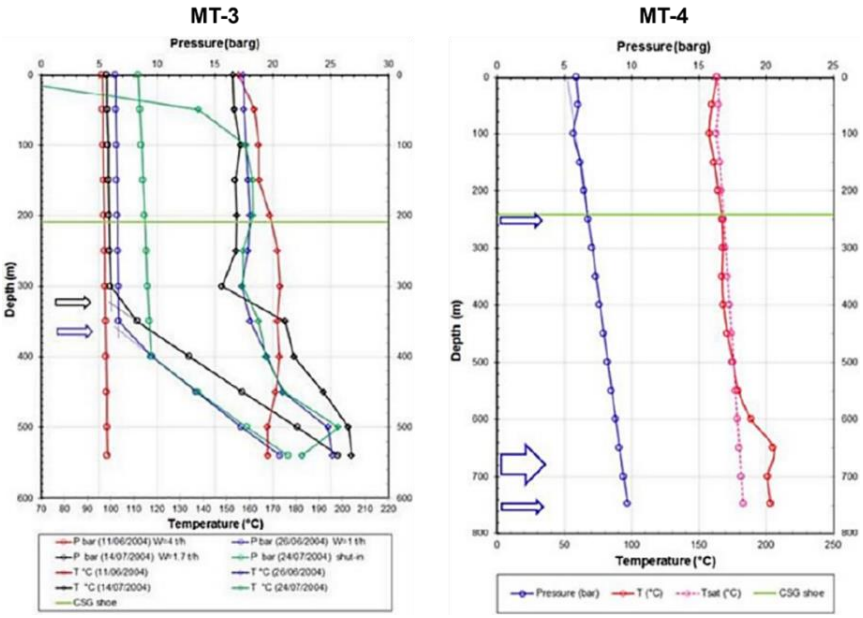

Figure 17: Pressure-Temperature Logs of MT-3 and MT-4 Wells (Wahyuningsih & Sitorus, 2004).

Meanwhile, the shut-in P-T log of MT-3 shows that the wellbore is filled by a steam column and water column with water column at the 400 m depth (562 masl). Conductive profile can be seen at the very shallow depths between 0-100 m since the heat transfer mode is dominated by the conduction of the clay cap. However, advective profile can be seen below the 100 m depth (863 masl). Furthermore, the highest recorded wellbore temperature by the shut-in P-T log was 198^{o}C at the depth of 540 m (423 masl). However, temperature reversal occurs at the 540 m, possibly due to horizontal or tilted high-temperature geothermal fluid flows in the subsurface (Wahyuningsih & Sitorus, 2004). Furthermore, the flowing P-T log of MT-4, shows that feed zones were encountered at the depths of 250 m (733 masl), 650 m (333 masl), and 747 m (236 masl). Between the depths of 550-747 m, the wellbore temperatures (179.4-205.5^{o}C) are higher than the saturation temperature at the corresponding pressure. This indicates that the feed zones at the depths of 650 m and 747 m supply superheated steam to the wellbore. However, the superheated steam forms a water column up to the 100 m depth. Consequently, the water column was pushed outside during well discharge, causing test separator flooding and disturbed the steam flow rate. These concluded MT-4 is not feasible to become a production well (Wahyuningsih & Sitorus, 2004).

3.3.3 MT-3 and MT-4 Well Flow Testing

Two well flow tests were applied to MT-3 and MT-4: short-term flow test using lip pressure method; and 2) long-term flow test using orifice plate method. MT-4 flow testing used a separator because MT-4 discharged two-phase fluid. The results of MT-3 and MT-4 long-term flow test data acquisition are shown in Figure 18. The well tests were conducted at various upstream pressure (Pu) values.

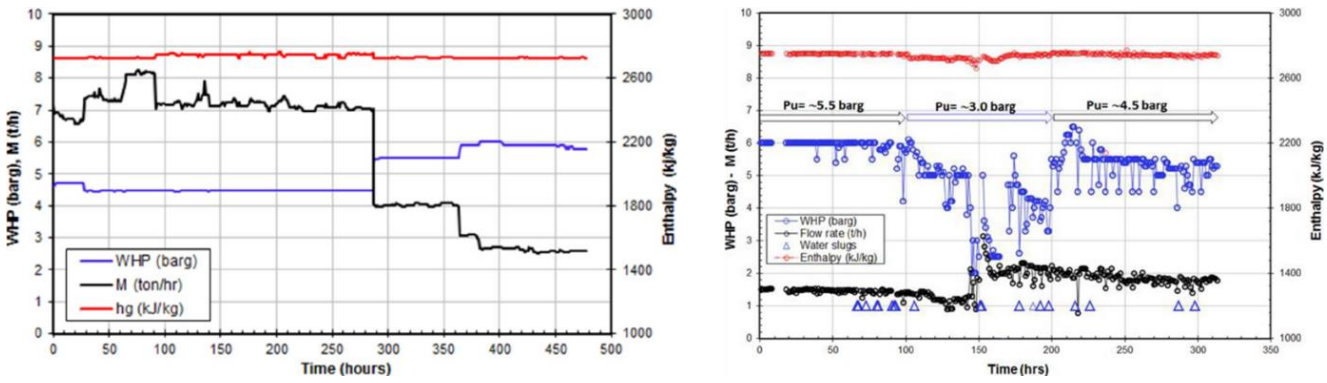

Figure 18: MT-3 Well Long-Term Flow Test Results at Pu = 3 barg (Left); MT-4 Long-Term Flow Test Results (Right) (Wahyuningsih & Sitorus, 2004).

The long-term flow test data of MT-3 are used to synthesize the deliverability curve of MT-3, as shown in Figure 19.Figure 19. Subsequently, calculation of the optimum operating condition to generate the highest well output was performed by assuming the turbine outlet pressure of 0.15 bara, turbine isentropic efficiency of 80%, and neglecting mass and heat losses. The results in show that MT-3 generates the highest output of 0.36 MWe at 4.5 barg WHP and discharges 2.89 tph of saturated steam with the enthalpy of 2727 kJ/kg. This WHP matches with typical minimum turbine inlet pressure for commercial condensing turbines of 5.5 bara (4.5 barg) (Suhanto &

Arsadipura, 2006). Meanwhile, MT-4 flow measurement were disturbed due to the well dicharging two-phase fluid with intermittent liquid slug flows that caused flooding of test separator flooding every 3-6 hours. The long-term flow test shows that the steam flow rate was 1.54-2.15 tph (liquid flow rate of 0.036 tph) at the Pu of 5.05-5.4 barg (WHP of 5.5-5.8 barg) (Wahyuningsih & Sitorus, 2004).

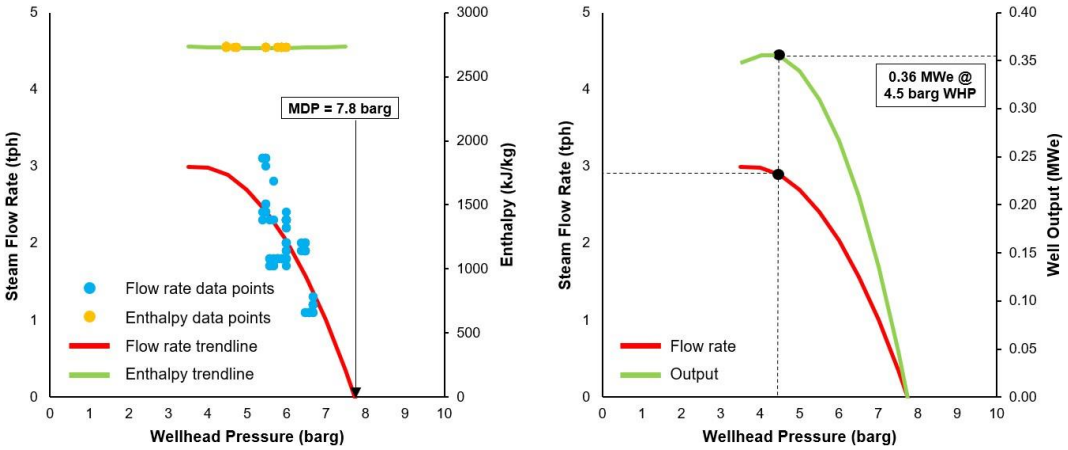

Figure 19: MT-3 Well Flow Rate and Enthalpy vs. WHP (Left); Flow Rate and Power Output vs. WHP (Right).

3.4 MT-5 and MT-6 Development Wells

3.4.1 MT-5 and MT-6 Drilling and Well Geology

Development drilling of MT-5 and MT-6 were performed in 2005 and 2006, respectively. Both wells used vertical standard hole-type. MT-5 was drilled at an elevation of 962 masl with a 378.2 m TVD. Meanwhile, MT-6 was drilled with a 123.8 m TVD. During MT-5 drilling, TLC occurred at depths of 155.5 m, 283 m, and 341 m. During MT-6 drilling, TLC occurred at the 42-124 m depths. This indicates that MT-5 and MT-6 well lithology is characterized by rocks with high permeabilty (Suhanto & Arsadipura, 2006). The well geology and casing design of MT-5 and MT-6 are shown in **Figure 21.** MT-6 well lithology consists of altered tuff breccia and altered andesite. Secondary minerals are dominated by iron oxide, clay minerals (kaolinite, smectite, and monmorilinite) with/without pyrite, calcite, secondary quartz, and anhydrite. The alteration intensity is medium-to-high. By considering the hydrothermal alteration types, MT-6 well lithology can be categorized into overburden (0-6 m depths or 956-962 masl) and argillic zone (6-378 m depths or 584-962 masl) that represents clay cap (Kasbani, et al., 2004).

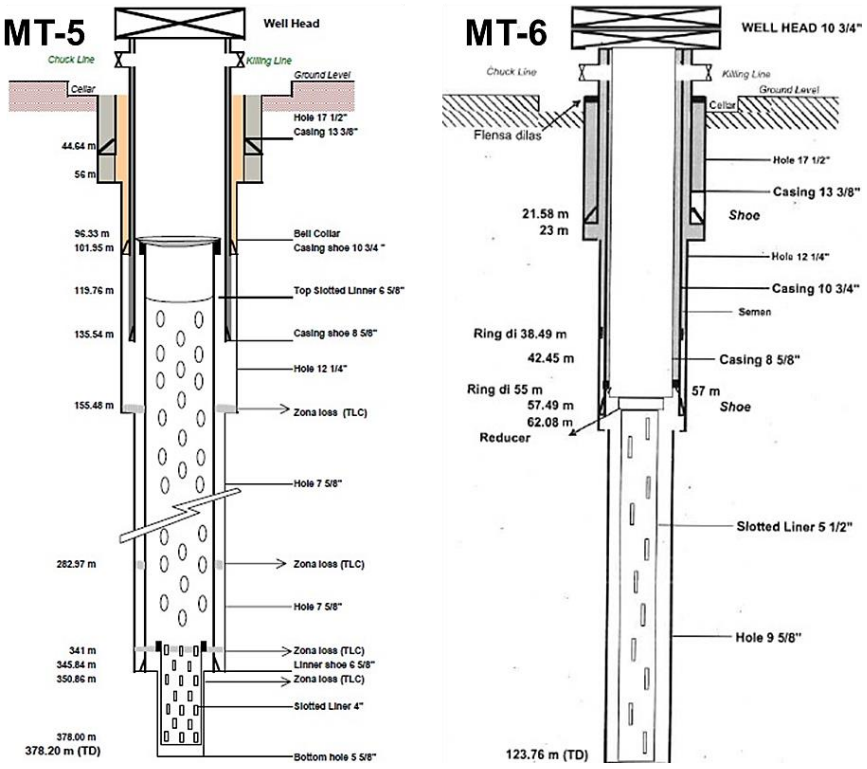

Figure 20: MT-5 and MT-6 Wells Geology and Casing Design (Suhanto & Arsadipura, 2006)**.**

3.4.2 MT-5 and MT-6 P-T Logging

Shut-in P-T logging were run twice at MT-2 well, as shown in Figure 21. The first shut-in P-T run shows that the highest downhole temperature was 152-156°C at the depths of 160-200 m. Meanwhile, the second shut-in P-T run shows that the highest downhole temperature was 169°C at 365 m depth (597 masl). Conductive profile only exists at the very shallow depths. Meanwhile, the P-T log mostly shows an isothermal and advective profile, which indicates that the feed zone of the discharged steam is possibly only at the bottomhole from a vapor-dominated reservoir (Suhanto & Arsadipura, 2006). The pressure build-up (PBU) test results show that the transmissivity under steady-state reservoir condition is 69.6 Darcy-meters and skin factor of -10.9, which characterizes a fracture zone. If the feed zone thickness is assumed to be 50 m, the permeability is 1.4 mD, which is a relatively high value (Suhanto & Arsadipura, 2006).

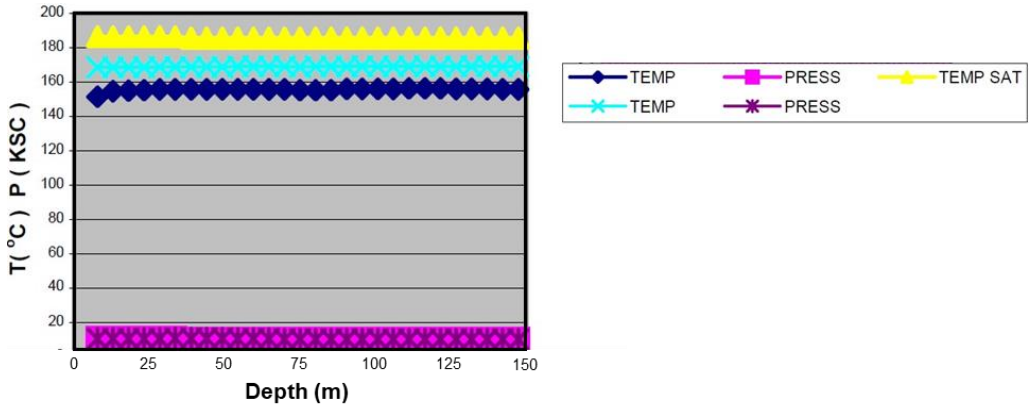

Figure 21: Shut-in Pressure-Temperature Logs of MT-5 Well (Suhanto & Arsadipura, 2006).

3.4.3 MT-5 Well Flow Testing

The well testing of MT-5 was performed at the WHPs of 4 kscg (3.9 barg), 5 kscg (4.9 barg), 6 kscg (5.9 barg), 7 kscg (6.9 barg), and 7.5 kscg (7.4 barg). The well discharged saturated steam. The well testing data of MT-5 are used to plot the deliverability curve of MT-5, as shown in Figure 22. Subsequently, calculation of the optimum operating condition to generate the highest well output was performed by assuming the turbine outlet pressure of 0.15 bara, turbine isentropic efficiency of 80%, and neglecting the mass and heat losses. The results in show that MT-5 generates the highest output of 2.24 MWe at the WHP of 3 barg and discharges 20.36 tph of saturated steam with the enthalpy of 2739 kJ/kg. However, the output at the WHP of 5.5 bara (4.5 barg) corresponding to typical minimum turbine inlet pressure for commercial condensing turbines is 2.12 MWe with the steam flow rate of 17.5 tph and enthalpy of 2752 kJ/kg. Meanwhile, the well flow testing of MT-6 shows that the well is not productive. Besides, MT-6 is located on a different morphology with MT-2, MT-3, MT-4, and MT-5 hence not affecting the previous wells. MT-6 also never experienced formation fluid influx/return flows despite more than 2 million litres of water and mud have been pumped into the well (Suparman, 2009).

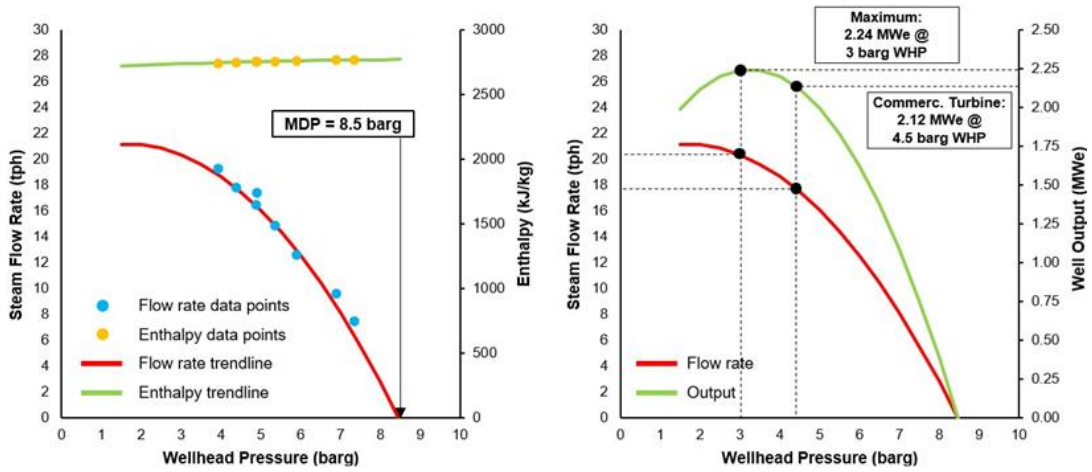

Figure 22: MT-5 Well Flow Rate and Enthalpy vs. WHP (Left); Flow Rate and Power Output vs. WHP (Right).

4. RESOURCE ASSESSMENT

4.1 Conceptual Model

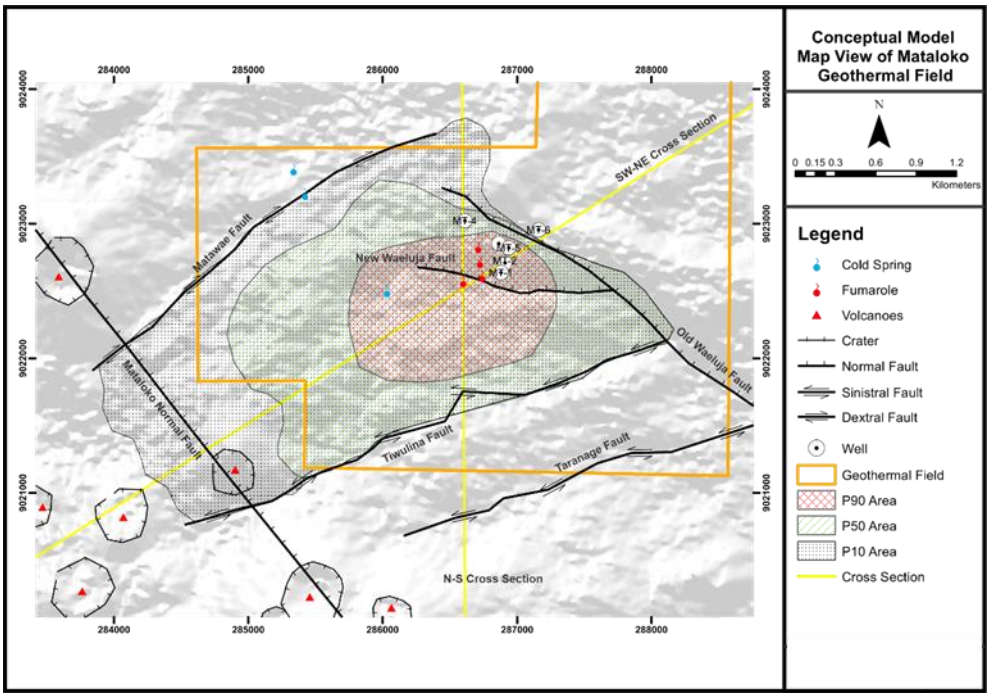

Figure 23: Mataloko Geothermal Field P10, P50, and P90 Prospect Area Distribution. Modified from (Jatmiko, et al., 2021).

The data used in the conceptual were reconnaissance survey data, 3G data, and drilling tests. From this data, a model is created that describes the cross section of the geothermal system describing geothermal components such as caprock, reservoir, heat source, fluid flow, discharge and recharge zone, upflow and outflow zone, as well as geological setting affecting geothermal field. In the Mataloko Geothermal Field, it is interpreted as a Low-Profile Geothermal System, characterized by slight relief differences assuming that the isothermal spreads laterally, so does the heat distribution. P90, P50, and P10 areas are comprehensively delineated and modelled to determine prospectus area of geothermal according to several parameters stated above as shown in Figure 23.

MT data were used to determine potential area of Mataloko geothermal field and its surrounding. In this case, area with low resistivity anomaly indicates the potential of geothermal resources. Hence, the P10, P50, and P90 are delineated by choosing area with MT anomaly. Permeability also has significant factor to review prospectus geothermal area to be delineated, presenting as the primary and secondary permeability. Generally, the lithologies formed in the study area are good enough to circulate geothermal fluid. However, the occurrence of fault can either result as the upflow pathway or outflow pathway since it can seal the lithologies so that it becomes the boundary of geothermal system. New Wae Luja Fault, located on the south part of MT-4 and west part of MT-2, has good secondary permeability shown by the occurrence of some manifestations, for instance fumarole and hot spring. Those manifestations display that this area is interpretably the upflow zone of Ratogesa geothermal system. Thus, P50 and P90 area is delineated by its occurrence of manifestations which directly correlate with upflow zone, as well as permeability caused by structures. In addition, the circulation of hydrothermal fluid and upflow zone indicate there is heat source below the system. Moreover, P90 is delineated according to proven area having geothermal resources and actively producing electric through the production well. On the other hand, Matawae Fault, Tiwulina Fault, and Taranage have impermeable fracture along its fault plane so that it functions as the boundary of geothermal system in this study area despite being new fault system. It is assumed that the impermeable layer on the fault plane is caused by strike-slip fault which produces fine-grain material which then is compacted and become impermeable. This factor underlies the reason on determining the boundary, the impermeable fault, of P50 in the south part of study area as well as P10, both south and north parts of the Mataloko geothermal field, specifically Ratogesa geothermal system. The delineation of P10 strecthly spreading to SW-NE direction is also related to geothermal system boundary of Matawae, Tiwulina, as well as Taranage Fault having impermeable fault fissure.

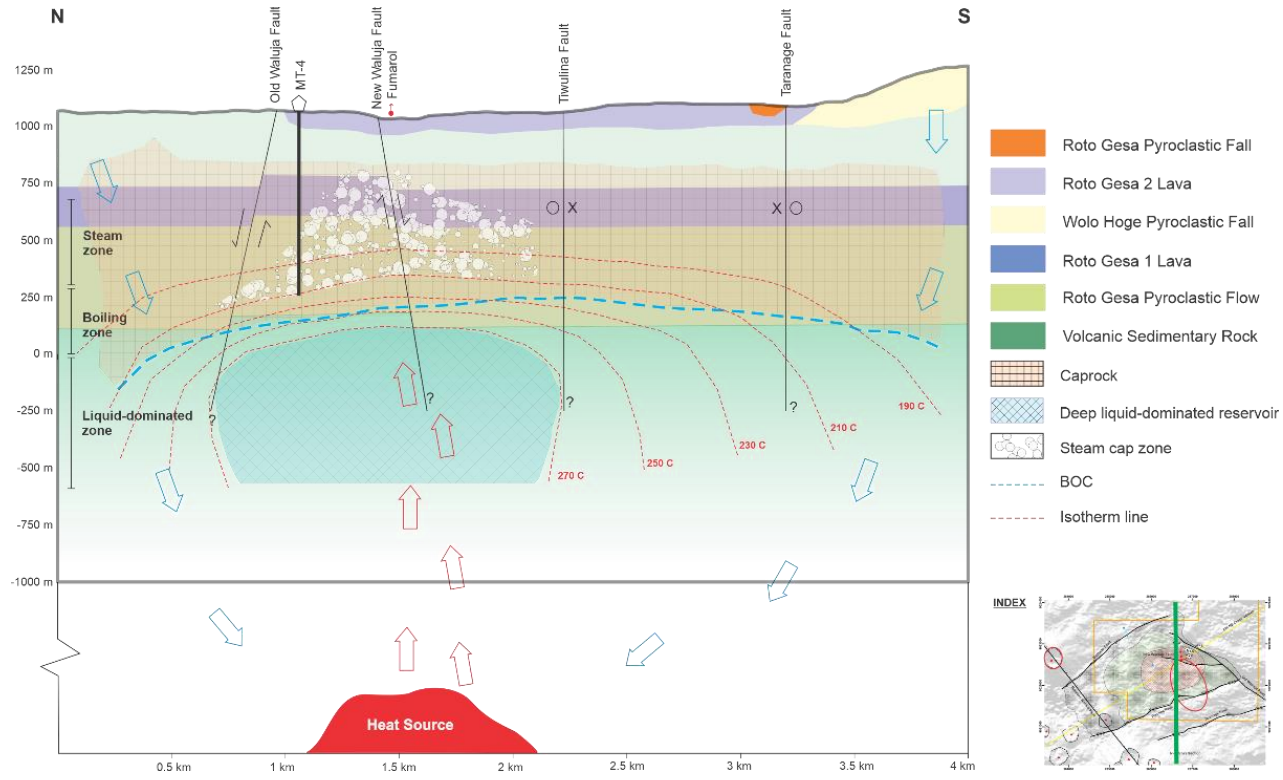

Figure 24: North-South Conceptual Model Cross Section.

N-S cross section shows subsurface model of Mataloko geothermal field. The upflow and the occurrence of deep liquid-dominated reservoir as well as the shallow vapor-dominated zone are strongly influenced by the New Wae Luja Normal Fault. New Wae Luja Normal Fault acts as the pathway of upflow in the study area, while the Old Wae Luja Normal Fault and Tiwulina Dextral Fault becomes the geothermal system boundary since it is impermeable as it is shown in Figure 24.

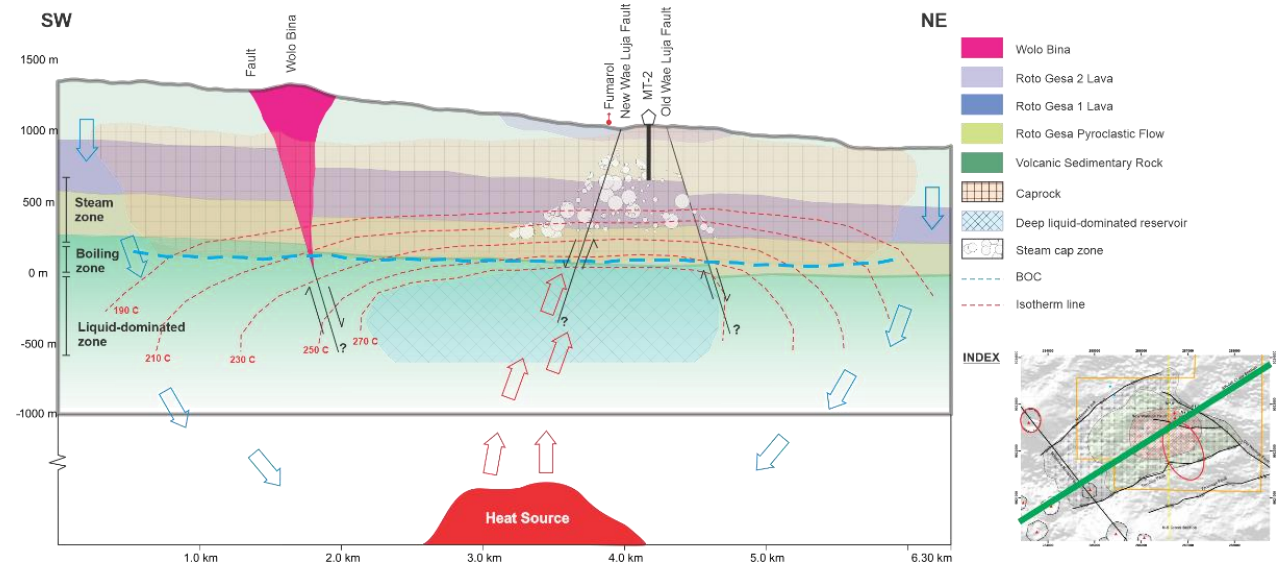

Figure 25: Southwest-Northeast Conceptual Model Cross Section.

SW-NE cross section also shows the same interpretation in which New Wae Luja Normal Fault plays as the upflow pathway and Old Wae Luja Normal Fault acts as the reservoir boundary in this system (Figure 25).

4.1.1 Reservoir Rock and Geothermal Fluid

Subsection Mataloko geothermal field is dominated by volcanic and volcaniclastic rocks having medium rock permeability. Products of old volcanic rock event and younger volcanic rock make up almost 1000 m in thickness. Therefore, the reservoir (liquid dominated) is interpreted to place the basement rock consisting of tuff and pyroclastic having medium permeability. The reservoir size is believed to be

controlled by impermeable fault plane. Meanwhile, the shallow-vapor dominated zone is within the cap rock. The elevation of shallow vapor-dominated and deep liquid-dominated zones is estimated by considering the elevation of feed zone, advective P-T profile, top of steam column, geochemistry estimation of isothermal line, alteration zone, and base of conductive, as shown in Table 3 and Table 4.

Table 3: Shallow Vapor-Dominated Zone Thickness Estimation.

Parameter	Value	Consideration
Top of Shallow Vapor-Dominated Zone		
Maximum	823 masl	• Shallowest steam feed zone encountered by MT-2 • Advective profile of shut-in P-T log of MT-3 and MT-5
Most likely	692 masl	Median of "maximum bottom" and "minimum bottom"
Minimum	562 masl	• Top of steam column based on shut-in P-T log of MT-3 • Advective profile of shut-in P-T log of MT-3 and MT-5
Bottom of Shallow Vapor-Dominated Zone		
Maximum	360 masl	• Geochemistry estimation of 210^{o}C isothermal line • Phylic and transitional zone encountered by MT-4
Most likely	300 masl	Median of "maximum bottom" and "minimum bottom"
Minimum	240 masl	• Geochemistry estimation of 230^{o}C isothermal line Propylitic zone encountered by MT-3 and MT-4
Shallow Vapor-Dominated Zone Thickness		
Maximum	583 m	"Maximum top" minus "minimum bottom"
Most likely	392 m	"Most likely top" minus "most likely bottom"
Minimum	202 m	"Minimum top" minus "maximum bottom"

Table 4: Deep Liquid-Dominated Zone Thickness Estimation.

Parameter	Value	Consideration
Top of Deep Liquid-Dominated Zone		
Maximum	50 masl	Base of conductive from MT interpretation
Most likely	0 masl	• Geochemistry estimation of 270^{o}C isothermal line • Resisitivity 15-50 Ω.m from MT interpretation
Minimum	-50 masl	Resistivity 15-50 Ω.m from MT interpretation
Bottom of Deep Liquid-Dominated Zone		
Most likely	-600 masl	Deepest feed zone of the deepest well in Sokoria field minus 200 m (as a benchmark to Mataloko field)
Deep Liquid-Dominated Zone Thickness		
Maximum	650 m	"Maximum top" minus "most likely bottom"
Most likely	600 m	"Most likely top" minus "most likely bottom"
Minimum	550 m	"Minimum top" minus "most likely bottom"

4.1.2 Heat Source

From alteration and manifestation at Mataloko Geothermal Field, it is interpreted that the heat soure are vertically beneath the surface. It is implied from the occurrence of alteration minerals indicating high sulfidation epithermal system. in this case, the fluids come directly from the subsurface, mainly in vertical direction. Besides, since geothermal field is located inside the Ratogesa Crater System, the heat source is suspectedly directly coming from Ratogesa Crater Magmatism.

4.1.3 Caprock

According to the resistivity method, the caprock is approximately 800 m thick. The caprock is intruded by Wae Luja fault, so there was a steam intrusion in the caprock.

4.1.4 Permeability Control

The permeability in Mataloko Geothermal Field is interpreted as medium permeability. Both primary and secondary permeability are important to geothermal fluid circulation. Obtained data and analysis show that the permeability is dominantly controlled by New Wae Luja Normal Fault. As a result, the high permeability is not evenly distributed. Eventhough fault is considered as fluid pathway, the other faults show the opposite which later in this case become geothermal fluid boundary. Based on the analysis, the liquid reservoir has medium to high permeability, since the lithology is pyroclastic materials and fault (New Wae Luja Normal Fault) mainly controls the upflow.

4.1.5 Upflow and Outflow

The upflow is distributed inside the Ratogesa Crater indicated by the occurrence of manifestations such as fumarole. The upflow also correlates to New Wae Luja Normal Fault directly affecting the fluid pathway. On the other hand, the outflow is located on the south-west area of Mataloko field having lower elevation.

4.1.6 Recharge Water

There are two fault lines that can be identified as the recharge zone which are located in the southwest and northeast of Mataloko, respectively. The southern-southwestern part of Mataloko is also potential to be a recharge zone since this area has high terrain that could transfer the meteoric water to the reservoir.

4.2 Resource Size Estimation

The estimate the resource size of Mataloko geothermal field, the volumetric stored heat method with Monte Carlo probabilistic simulation is applied. Due to the existence of distinctive shallow vapor-dominated and deep liquid-dominated zones, the volumetric stored heat calculation for each zone is performed separately. The input values for the calculation are shown in Table 5.

Table 5: Monte Carlo Simulation Input Parameters.

Parameter	Unit	Shallow Vapor-Dominated			Deep Liquid-Dominated			Source
		Min	Most Likely	Max	Min	Most Likely	Max	
Area	km^2	0.8	1.4	4.1	1.4	6.5	4.1	Well and 3-G data
Thickness	m	171	374	577	500	550	600	Well and 3-G data
Rock density	kg/m^3	2650	-	-	2650	-	-	Indonesia National Standard 6482:2018
Porosity	fract.	0.1	0.12	0.13	0.07	0.075	0.08	(Pradhipta, et al., 2019)
Rock specific heat	kJ/kg^oC	0.9	1.05	1.1	0.95	0.98	1.0	(Pradhipta, et al., 2019)
Lifetime	year	30	-	-	30	-	-	Indonesia National Standard 6482:2018
Recovery factor	fract.	0.25	0.5	0.45	0.22	0.23	0.25	(Muffler & Cataldi, 1978)
Electrical efficiency	fract.	0.12	0.14	0.16	0.09	0.10	0.12	(Zarrouk & Moon, 2014)
Initial temperature	^oC	175	205	230	270	288	306	Well and 3-G data
Cut-off temperature	^oC	180	-	-	180	-	-	Indonesia National Standard 6169:2018
Init. water saturation	fract.	0.1	0.3	0.4	0.93	0.95	1.0	(Pradhipta, et al., 2019)
Final water saturation	fract.	0.0	0.05	0.1	0.3	0.4	0.5	(Pradhipta, et al., 2019)

The results of Monte Carlo simulation are shown in Figure 27. The resource size of the shallow vapor-dominated zone is 0.75 MWe (P10), 3.01 MWe (P50), and 6.93 MWe (P90). Meanwhile, the resource size of the deep liquid-dominated reservoir is 13.25 MWe (P10), 22.14 MWe (P50), and 31.48 MW (P90). The P50 resource size is recommended to become the moderate basis of power plant capacity selection.

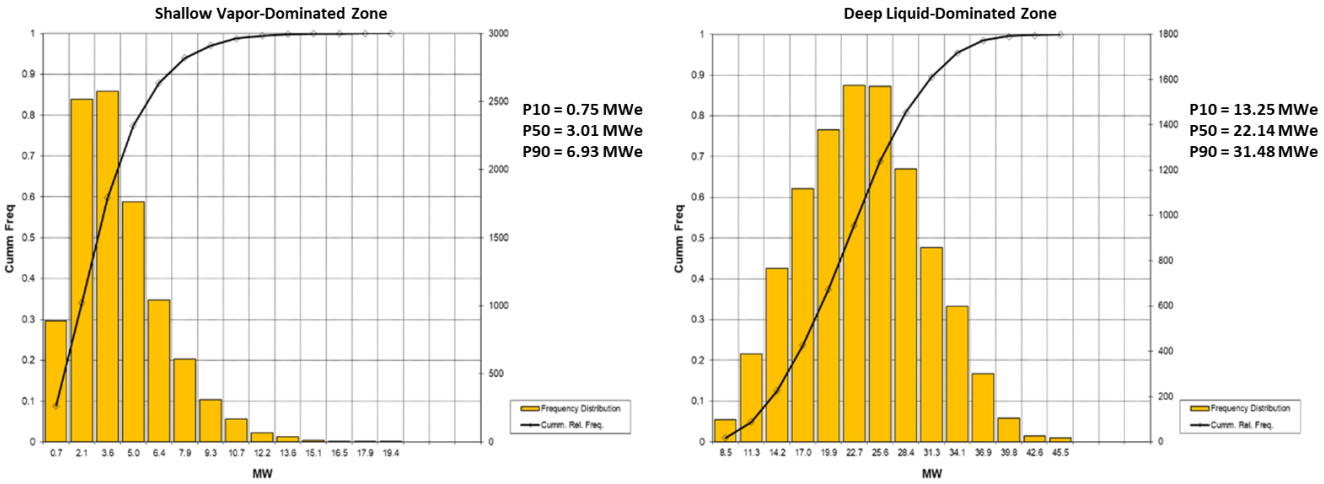

Figure 26: Histogram of Monte Carlo Simulation Results.

5. FIELD DEVELOPMENT

5.1 Field Development Strategy

This study proposed in-stages development of Mataloko geothermal field by utilizing both reservoir zones (shallow vapor-dominated and deep liquid-dominated) with the total installed capacity of 22 MWe. This consists of 2 MWe production from the shallow vapor-dominated zone and 20 MWe production from the deep liquid-dominated zone using two scenarios, as shown in , considering the technical and economic aspects. The P50 resource size (3.01 MWe for shallow vapor-dominated zone and 22.14 MWe for deep liquid-dominated zone) is employed as the reference for the power plant size to increase the probability that the geothermal power generation could sustain for up to 30 years. Additionally, in-stages development mitigate the risk of oversizing the capacity of the first installed power plant unit that may cause the reservoir to shock hence causing rapid reservoir depletion which could lead to unsustainable production. Furthermore, a single-unit power plant with large capacity increases the financing risk by concentrating the investment at the early stage of the project despite being under the uncertainty of the resource's capacity. In-stages development may also alleviate the impact of negative present values at the early stage of the project by distributing the investment at the middle of the project.

Table 6: Mataloko Geothermal Field 22 MWe Installed Capacity Development Scenarios.

Power Plant Unit	Installed Capacity (MWe)	COD	Productive Reservoir Zone Target
Scenario 1			
Unit 1	2	2025	Shallow vapor-dominated (already drilled)
Unit 2	20	2033	Deep liquid-dominated
Scenario 2			
Unit 1	2	2025	Shallow vapor-dominated (already drilled)
Unit 2	10	2029	Deep liquid-dominated
Unit 3	10	2033	Deep liquid-dominated

5.2 Development Drilling Strategy

Since development drilling have been done in the shallow vapor-dominated and MT-3 and MT-5 wells are capable to generate 2 MWe, the subsequent development drilling strategy targets the deep liquid-dominated zone. By assuming the output of 6 MWe/well and reinjection-production ratio of 57% (International Finance Corporation, 2013), 4 production and 2 reinjection wells are needed. By considering the drilling success rate of 70%, 6 production and 3 reinjection well drillings are needed.

5.2.1 Well Targeting

Production well targeting is performed on the constructed conceptual model, as shown in Figure 27 by considering subsurface and surface considerations. The subsurface considerations are: 1) upflow zone; 2) permeable faults; 3) high temperature (> 225°C); and 4) non-acidic area. Meanwhile, surface considerations are: 1) low geohazard risk area, such as landslide and volcanic eruption; 2) access to existing infrastructure and drilling water sources; and 3) appropriate land function (Purba et al., 2019). The drilling sequence starts from the production well target that has highest confidence of success inside P90 area, which is MTA-1 well, then step out to the reservoir boundaries and followed by reinjection drilling.

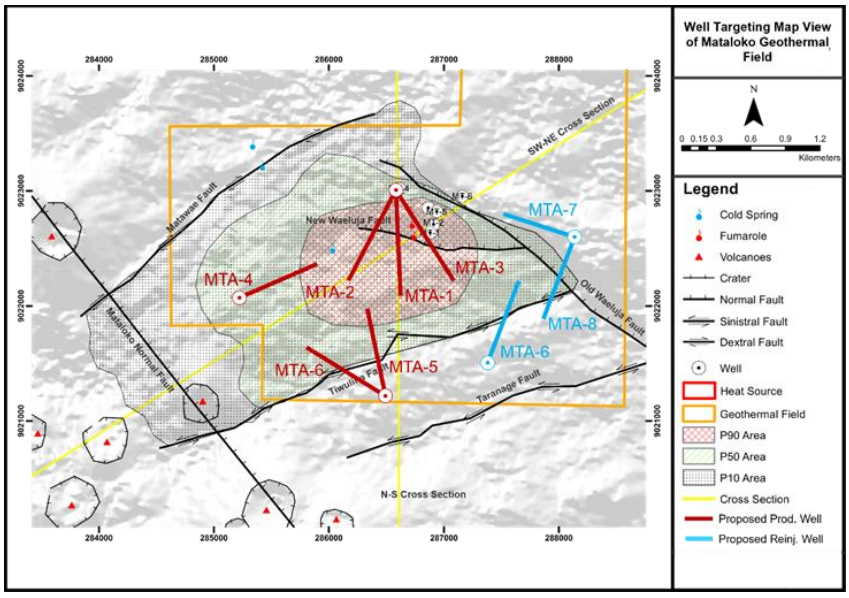

Figure 27: Well Targeting Plan.

5.2.2 Well Type Selection

Due to the small diameter, slimhole is not suitable for development drilling. For the subsequent development drilling, GeoMech Inc. suggest using directional standard hole by considering: 1) directional well enables getting larger primary and secondary permeability zones; 2) the subsurface lithology is dominated by pyroclastic sediment rocks, which are less hard than crystalline rocks, thus enabling directional standard hole drilling; 3) standard hole needs less area and cost than bigger hole, leading to less environmental footprint and financial risk.

5.2.3 Directional Well Trajectory

The planned production wells use directional well. The well trajectory is calculated referring to (Omar, 2013) and the results are shown in Table 7. The KOP starts at 100 mMD and the target is at 1644.4 mMD with the max. inclination of 35.6°.

Table 7: Well Trajectory Calculation.

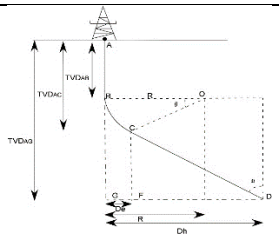

Parameter	VD (m)	Horizontal Displ. (m)	MD (m)
KOP	100	0	100
EOB	433.6	107.1	456
Target	1400	800	1644.4
Max. inclination (θ)		35.6°	
Buildup rate (BUR)		3°/30 m	
Radius of curvature (R)		573 m	

Calculation

Radius of Curvature

$R = \frac{180}{\pi} \times \frac{1}{BUR}$

$R = \frac{180}{\pi} \times \frac{1}{3^o/30} =$ **573 m**

End of Build

$MD = TVD_{AB} + \frac{\theta}{BUR} == 100 + \frac{35.6^o}{3^o/30} =$ **456 m**

$VD = TVD_{AB} + R\sin\theta = 100 + 573\sin(35.6^o) =$ **433.6 m**

$Horiz.\ displ. = R \times (1 - \cos\theta) = 573 \times (1 - \cos(35.6^o)) =$ **107.1 m**

Target

$MD = TVD_{AB} + \frac{\pi \times \theta \times R}{180^o} + \frac{TVD_{AG} - TVD_{AB} - R\sin\theta}{\cos\theta} = 100 + \frac{\pi \times 35.6^o \times 573}{180^o} + \frac{1400 - 1000 - 573\sin(35.6^o)}{\cos(35.6^o)} =$ **1644.4 m**

5.2.4 Casing Schematic

The casing setting depth to reach the target at 1400 mTVD is determined based on BPD as the lower limit and fracture pressure as the upper limit assuming the fracture gradient of 0.63 psi/ft and water table up to 100 m depth, as shown in Figure 28. Furthermore, the casing and hole diameter are chosen based on NZS 2403:2015.

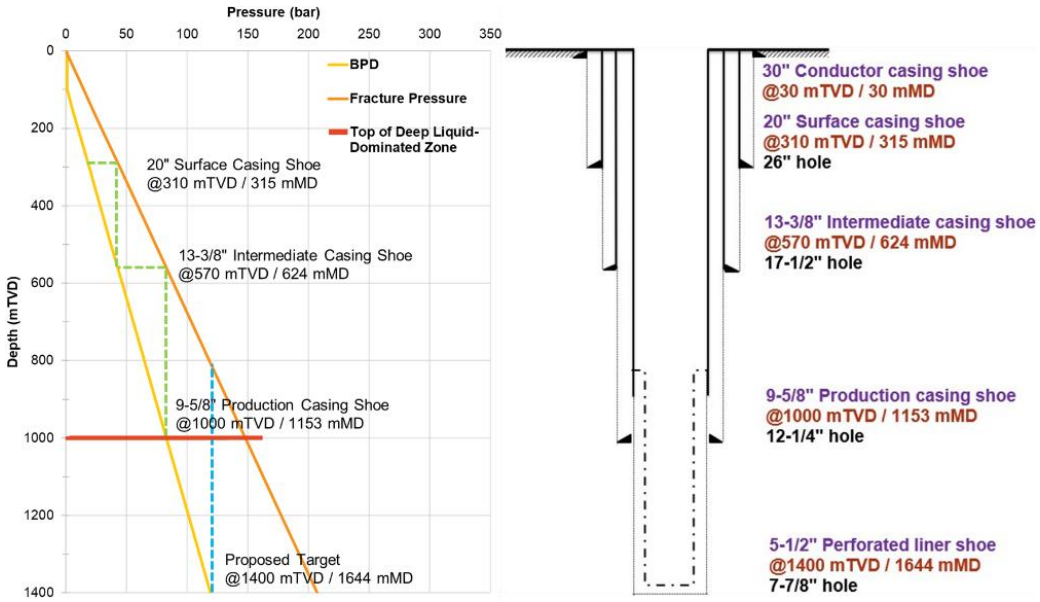

Figure 28: Well Design and Casing Depth Casing.

5.2.5 Drilling Prognosis

The production well drilling prognosis is shown in Figure 29. The lithologies that will be penetrated are Roto Gesa 2 Lava, Roto Gesa Pyroclastic Flow, Roto Gesa 1 Lava, and Volcanic-Sedimentary Rock. In the claycap zone, argillic alteration minerals exist and smectite clay swelling could occur and cause wellbore instability leading to stuck pipe. PLC and TLC is expected to occur since the caprock zone near Wae Luja fault's fracture zone down to the deep liquid-dominated zone.

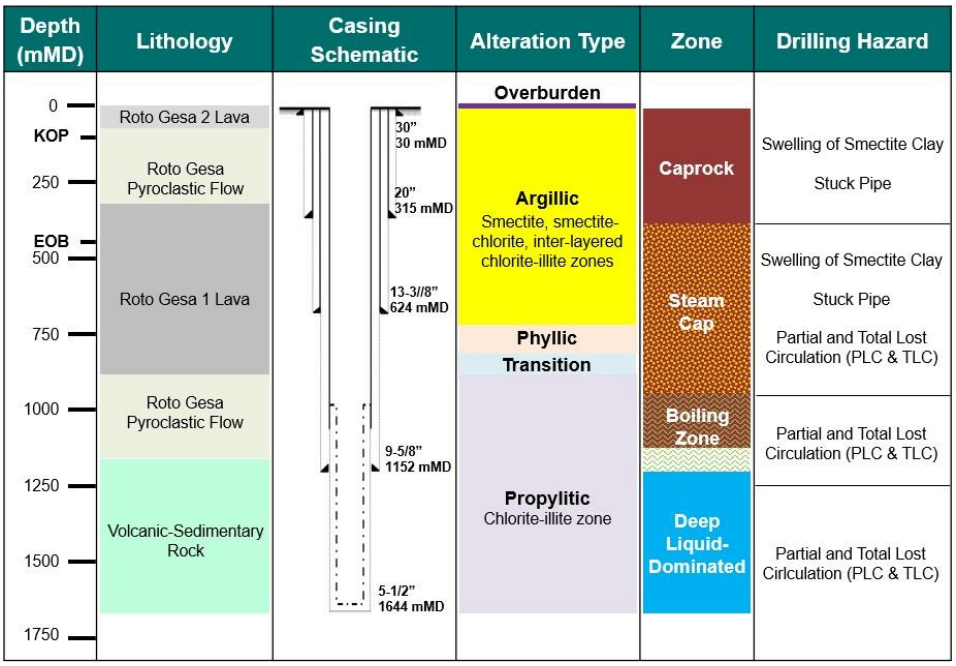

Figure 29: Drilling Prognosis.

5.2.6 Drilling Duration

The estimated required drilling time to reach the target at 1644.4 mMD is 37 days, as shown in Figure 30. The drilling of each well section involves hole drilling, trip to shoe, hole cleaning, pull out of the hole (POOH), casing running, and cementing.

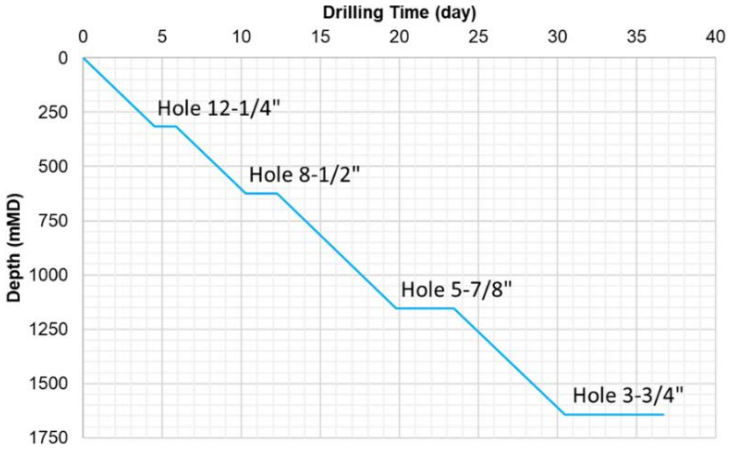

Figure 30: Drilling Depth vs. Duration.

5.3 Power Plant

5.3.1 Power Plant Technology Selection

This study proposed using direct steam (condensing) power plant for the 2 MWe generation from the shallow vapor-dominated and single-flash (condensing) for the 20 MWe generation from the deep liquid-dominated zone. Dry steam or vapor-dominated reservoirs including Mataloko's shallow vapor-dominated zone is only suitable for direct steam power plants. Meanwhile, liquid-dominated reservoir may use flash-steam (single or double-flash) or combined flash-binary plant. Additionally, single-flash power plant enables brine reinjection at a higher temperature and pressure than double-flash or combined flash-binary plant, which is better for reservoir management. Furthermore, the investment costs for single-flash (1.8 million USD/MW) is cheaper than double-flash (2.1 million USD/MW) due to simpler equipment (Zeyghami, 2010).

5.3.2 Power Plant Preliminary Design

Mataloko GPP Unit 1 (2 MWe direct-steam) is designed based on the performance of MT-3 and MT-5. Meanwhile, Unit 2-3 (20 MWe single-flash) is designed in analog with other Indonesian high-temperature geothermal fields that produces fluids from a liquid-dominated reservoir below a steam cap (Ulum, et al., 2017). The preliminary power plant design is shown in Figure 31 and Table 8.

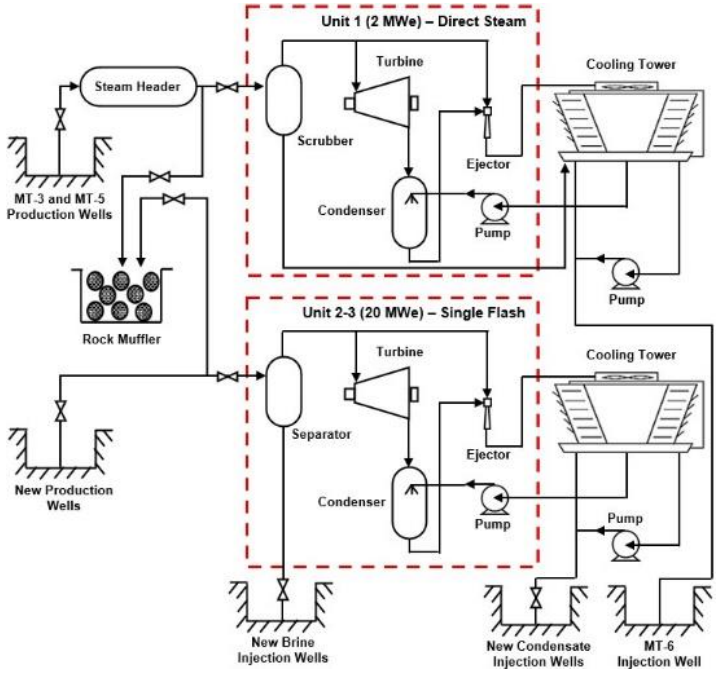

Figure 31: General Schematic of the Proposed Mataloko Geothermal Power Plant.

Table 8: Calculated Mataloko Geothermal Power Plant Operating Conditions.

Component	Parameter	Unit 1 (2 MWe) Direct Steam	Unit 2-3 (20 MWe) Single-Flash	Unit
Production well	Wellhead pressure	6.5	11	bara
	Fluid flow rate	4.68	179.6	kg/s
	Vapor fraction	100%	20%	-
Separator	Separator pressure	No separator	7	bara
	Vapor fraction	No separator	23.7%	-
Turbine	Type	Condensing	Condensing	-
	Turbine inlet pressure	6	6.5	bara
	Steam flow rate	4.68	43.5	kg/s
	Isentropic efficiency	80%	80%	-
	Specific steam consumption	2.30	2.07	kg/MW.s
Generator	Generator efficiency	95%	95%	-
Condenser	Condenser pressure	0.15	0.15	bara
Reinjection well	Brine flow rate	No brine	136.1	kg/s
	Brine temperature	No brine	164.1	^{o}C
	Condensate flow rate	4.68	43.5	kg/s

5.4 Fluid Collection and Reinjection System (FCRS)

There are 3 types of separator station: wellpad, satellite, and centralized (DiPippo, 2016). We suggest wellpad-centralized hybrid separator for Unit 2-3 by considering the land morphology in Mataloko geothermal field and the proposed well pad locations. Such FCRS design has been implemented in Ulubelu geothermal field (Mubarok & Zarrouk, 2016). Several factors are considered while determining the FCRS route, such as avoiding uphill two-phase flow from production wellhead to power plant, routing the pipeline over moderate slope terrain to ease installation, avoiding landslide areas and crossing water flows that are eroding, using gravity-aided reinjection where possible, and minimizing pipeline length to reduce pressure drops, cost, civil works, and environmental land use. Meanwhile, the determination of power plant location also considers the factors as listed in Table 9.

Table 9: Power Plant Location Considerations.

Condition	Appropriate	Innapropriate	Source
Forest type	Protected, production	Conservation	Indonesian Law No. 41/1991 and Indonesian Govt. Reguation No. 24/2010
Slope	0-40%	> 40%	Indonesian Ministry of Public Works Regulation No. 41/PRT/M/2007
River	> 200 m from riverbank	0-200 m from riverbank	Indonesian Govt. Regulation No. 38/2011
Fault	> 200 m from fault	0-200 m from fault	(Yousefi & Ehara, 2008)
Vegetation density	Low-moderate	High	(Noorollahi, 2005)
Primary road	> 100 m from primary road	0-100 m from primary road	Yousefi & Ehara (2008)
Settlement	> 500 m from settlement	0-500 m from settlement	Indonesian Ministry of Public Works Regulation No. 41/PRT/M/2007
Geothermal prospect zone	0-3 km from prospect zone	> 3 km from prospect zone	(Yousefi & Ehara, 2008)
Manifestation	> 100 m from manifestaion	0-100 from manifestation	(Yousefi & Ehara, 2008)

Furthermore, the proposed schematic of Mataloko geothermal field FCRS is shown in Figure 32.

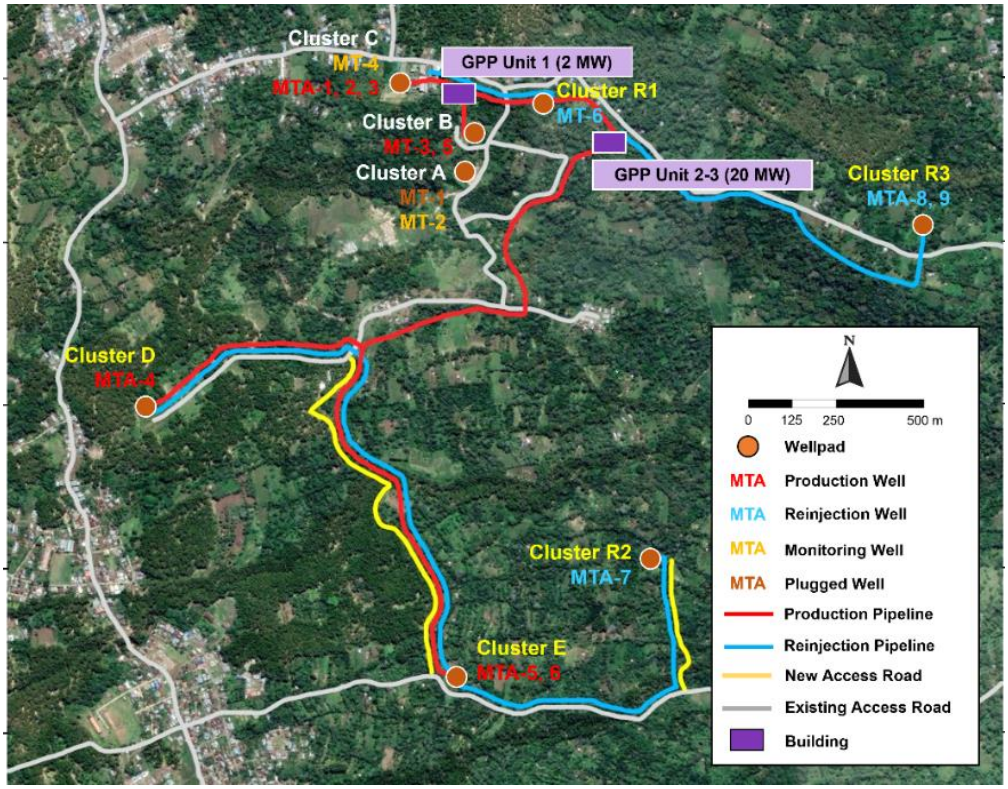

Figure 32: Proposed Schematic of Mataloko Geothermal Field FCRS.

5.5 Make-Up Well

By assuming 4% decline rate and the well outputs for steam cap and deep liquid-dominated zones are 1.5 MWe/well and 6 MWe/well, respectively, both scenarios require 6 make-up wells. By considering the make-up drilling success ratio of 80%, 8 make-up drillings are required, as shown in Table 10. The make-up well drilling will be required every 5-6 years on average.

Table 10: Summary of Production Well Make-Up Requirements.

Productive Reservoir Zone	Scenario 1		Scenario 2	
	Required	Drilled	Required	Drilling
Shallow vapor-dominated	2	3	2	3
Deep liquid-dominated	4	5	4	5
Total	**6**	**8**	**6**	**8**

6. PROJECT ECONOMICS

6.1 General Schedule of the Project

Since 2 exploration, 2 delineation, and 2 steam cap development wells have been drilled, we exclude the economic evaluation of 3-G surveys, exploration drilling, and steam cap development drilling. The project will start from 2024 with the steam cap development and will be continued by liquid-dominated reservoir development. The project timelines for Scenario 1 (2+20 MWe) and Scenario 2 (2+10+10 MWe) are shown in Figure 33, respectively.

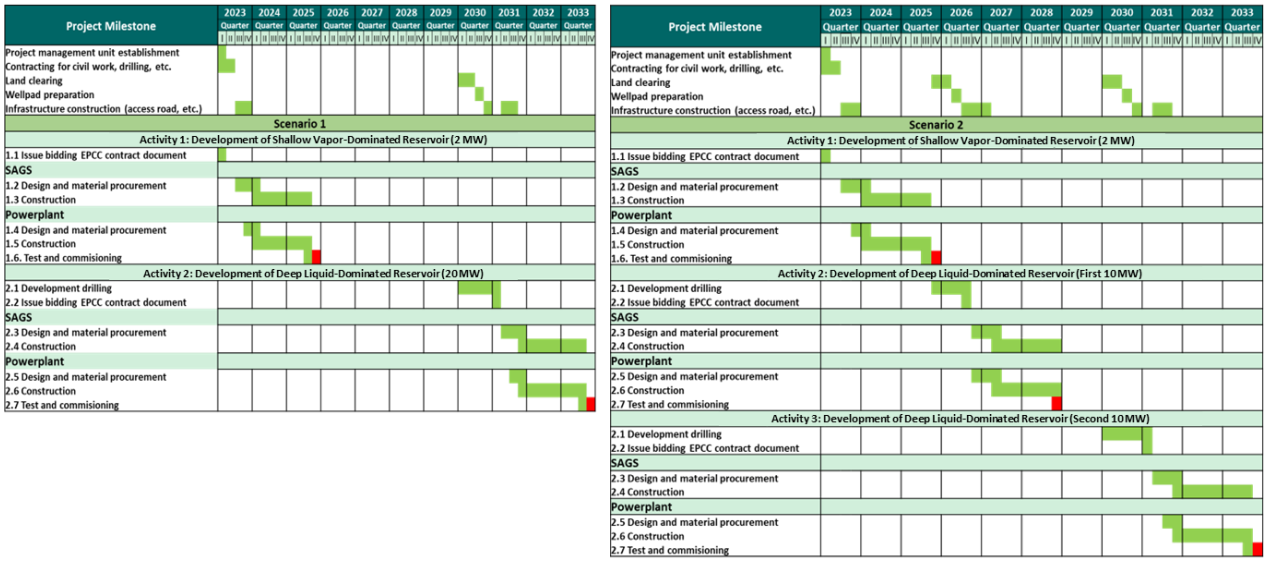

Figure 33: Project Schedule for Scenarios 1 and 2.

6.2 CAPEX, OPEX, and Other Financial Modeling Variables

The capital expenditure (CAPEX) and operating expenditure (OPEX) calculation results are shown in Table 11. The CAPEX is the same for both development scenarios, which is 102.9 million USD (4.7 million USD/MW), since there are no differences in CAPEX component, such as wells. The biggest CAPEX share is the development drilling (50%), which includes the production well drilling, injection well drilling, and make-up well drilling. The subsequent biggest CAPEX share is the power plant, SAGS, and interconnection. The total cost for the project approximately around 102.3 million USD for 22 MWe development (4.67 million USD/MWe).

Table 11: CAPEX and OPEX Calculation Results.

Cost Component	Unit Cost (USD)	Unit	Reference	Required	Total Cost (USD)
CAPEX					
Feasibility study	100,000	MW	(UNFCCC/CCNUCC, 2012)	22	2,200,000
Land acquisition and civil works	2,000,000	Activity	(Lesmana, et al., 2020)	1	2,000,000
Production well	5,755,000	Well	(Lesmana, et al., 2020)	6	34,527,000
Reinjection well	5,755,000	Well	(Lesmana, et al., 2020)	3	16,361,000
FCRS	350,000	MW	(Wahdjosoedibjo & Hasan, 2018)	3	7,700,000
Electrical substation	320,000	MW	(ESMAP, 2012)	22	7,040,000
Power plant EPCC	1,800,000	MW	(ESMAP, 2012)	22	33,000,000
				Total CAPEX	**102,829,000**
				CAPEX/MW	**4,674,000**
OPEX					
FCRS O&M	50,000	MW	(Lesmana, et al., 2020)	22	1,100,000
Power plant O&M	50,000	MW	(UNFCCC/CCNUCC, 2012)	22	1,100,000
Make-up well	5,755,000	Well	(Lesmana, et al., 2020)	8	46,036,000
Adm. management	30,000	MW	(Henneberger, 2013)	22	660,000
				Total OPEX	**48,896,000**
				Average Annual OPEX	**1,287,000**

Additionally, other financial modeling variables that are required in the analysis are summarized in Table 12.

Table 12: Other Financial Modeling Variables.

Variable	Value	Source
Tangible cost	30%	(Kivure, 2015)
Depreciation period	8 years	Indonesian Ministry of Finance Regulation No. 21/2010
Depreciation rate	25%	Indonesian Ministry of Finance Regulation No. 21/2010
Debt-to-equity ratio	70:30	(Quinlivan, 2015)
Debt period	20 years	(Quinlivan, 2015)
Interest	4%	World Bank (2022)
Income tax	25%	Indonesian Law No. 36/2008
Discount rate	10%	(Winofa, et al., 2019)
Investment tax allowance (for 6 years)	5%	Indonesian Ministry of Finance Regulation No. 21/2010
Production bonus	0.5%	Indonesian Government Regulation No. 28/2016

6.3 Economic Analysis Results

Field development Scenario 1 (2+20 MWe) and Scenario 2 (2+10+10 MWe) are compared economically. The results in Table 13 show that, while both scenarios are economically feasible due to the positive NPV and IRR higher than discount rate, Scenario 2 is more economically viable than Scenario 1 with higher project NPV (18.6 million USD) and higher project IRR (19%). Additionally, the payback period for Scenario 2 is faster than Scenario 1 based on the cumulative discounted cashflow in Figure 34.

Table 13: Economic Analysis Results Comparison Between Scenarios 1 and 2.

Parameter	Scenario 1 (2+20 MWe)	Scenario 2 (2+10+10 MWe)
CAPEX	102,829,000 USD	102,829,000 USD
CAPEX/MW	4,674,000 USD/MW	4,674,000 USD/MW
NPV project	15,436,000 USD	18,612,000 USD
NPV equity	42,239,000 USD	40,582,000 USD
IRR project	16%	19%
IRR equity	52%	62%
Payback period	8.5 years	6 years

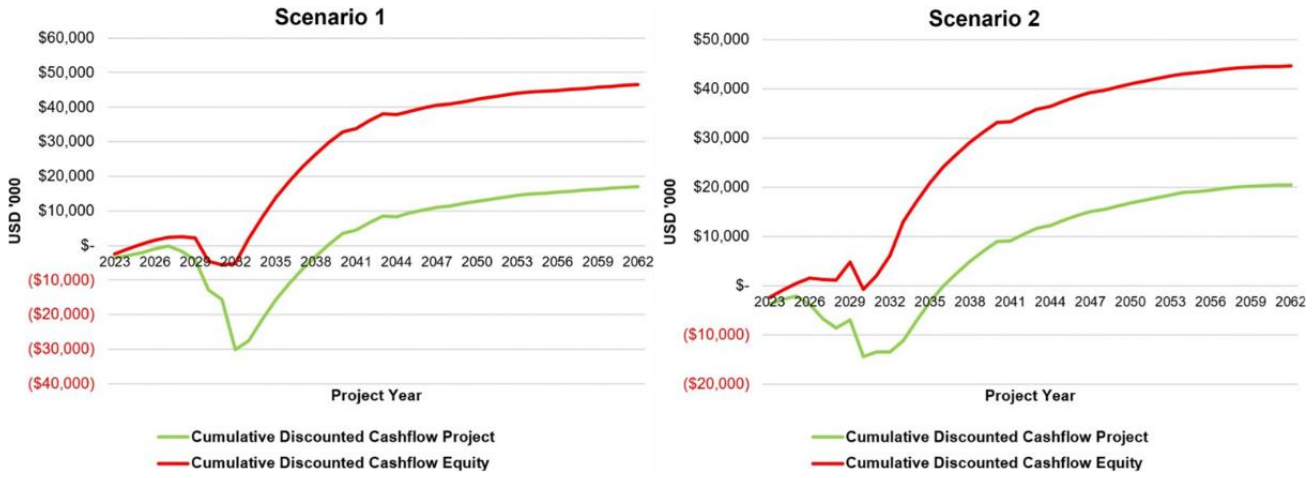

Figure 34: Cumulative Discounted Cash Flows for Scenarios 1 and 2.

7. CONCLUSION

Mataloko geothermal reservoir has two main zones: shallow vapor-dominated and deep liquid-dominated. The deep reservoir is predicted to be medium-high and controlled by secondary permeability from the Wae Luja fault. The geothermal fluid is predicted to be non-acidic and have low NCG content. The proposed stepwise development of 22 MWe installed capacity consists of 2 MWe production from the steam cap zone and 20 MWe production from the deep liquid-dominated zone using two scenarios: Scenario 1 (2+20 MWe) and Scenario

2 (2+10+10 MWe). The 2 MWe power generation from the steam cap will be supported by MT-3 and MT-5 wells, while the 20 MWe production from the deep liquid-dominated reservoir will require six production and three reinjection well drillings using directional standard holes. The economic analysis suggests Scenario 2 is more economically viable, requiring 102.9 million USD investment and yielding a project IRR of 19%, project NPV of 18.6 million USD, and a payback period of 6 years. The Mataloko field is technically and economically feasible to develop due to its medium-high permeability, high temperature, benign fluid, positive NPV, and IRR bigger than the discount rate.

REFERENCES

Ahmad, A. H., Adityatama, D. W., Rusdianto, M. A., Pradana, G. M., Beryll, T. A., Prasetyo, P. V., & Rachamadani, A. (2022). Geothermal Direct Use Alternatives in Mataloko to Increase Public Acceptance. *IOP Conference Series: Earth and Environmental Science, 1014*, 012010.

D'Amore, F., & Panichi, C. (1987). Geochemistry in Geothermal Exploration. In M. Economides, & P. Ungemach (Eds.), *Applied Geothermics* (pp. 69-89). New York: Wiley & Sons.

DiPippo, R. (2016). *Geothermal Power Plants Principles, Applications, Case Studies, and Environmental Impact.* Oxford: Elsevier.

Dwipa, S., Uchida, T., Yasukawa, K., Honda, M., & Andan, A. (2001). Integrated Geophysical Exploration in Mataloko Geothermal Area, Central Flores - East Nusa Tenggara. *Proceedings, INAGA Annual Scientific Conference & Exhibitions 2001*. Jakarta: International Geothermal Association.

ESMAP. (2012). *Geothermal Handbook: Planning and Financing Power Generation.* Washington, D.C.: Energy Sector Management Assistance Program.

Fauziyah, Y. H., & Daud, Y. (2019). Reconstruction of Conceptual Model in Mataloko Geothermal Field (Nusa Tenggara Timur). *Journal of Physics: Conference Series, 1341*, 082042.

Giggenbach, W. F., & Stewart, M. K. (1982). Process Controlling the Isotopic Composition of Steam and Water Discharges from Steam Vents and Steam-Heated Pools in Geothermal Areas. *Geothermics, 11*, 71-80.

Henneberger, R. (2013). Costs and Financial Risks of Geothermal Projects Geothermal Exploration. Istanbul: Best Practice Launch Event.

Indonesian Directorate General of Electricity. (2021). *Electricity Statistics Year 2020.* Jakarta: Indonesian Directorat General of Electricitiy Ministry of Energy and Mineral Resources.

Indonesian National Electricity Company. (2021). *Electricity Provision Business Plan (RUPTL) 2021-2030.* Jakarta: PT PLN (Persero).

International Finance Corporation. (2013). *Success of Geothermal Wells: A Global Review.* Pennsylvania: The World Bank.

Jatmiko, B. W., Pratama, H. B., & Sutopo. (2021). Updated Numerical Model of Mataloko Geothermal Field. *IOP Conference Series: Earth and Environmental Science, 732*, 012024.

Kasbani, Wahyuningsih, R., & Sitorus, K. (2004). Subsequent State of Development in the Mataloko Geothermal Field, Flores, Indonesia. *Proceedings of the 6th Asian Geothermal Symposium* (pp. 101-106). Daejeon: Korea Institute of Geoscience and Mineral Resources.

Kivure, W. (2015). *Geothermal Well Drilling Costing: a Case Study of Menengai Geothermal Field.* Kenya: Short Course X on Exploration for Geothermal Resources.

Lesmana, A., Winofa, N. C., Pratama, H. B., Ashat, A., & Saptadji, N. M. (2020). Preliminary Financial Modelling with Probabilistic Approach for Geothermal Development Project in Indonesia. *IOP Conference Series: Earth and Environmental Science, 417*(1), 012024.

Matsuda, K., Sriwana, T., Primulyana, S., & Futagoishi, M. (2002). Chemical and Isotopic Studies of Well Discharge Fluid of the Mataloko Geothermal Field, Flores, Indonesia. *Bulletin of the Geological Survery of Japan, 53*(2/3), 343-353.

Mubarok, M. H., & Zarrouk, S. J. (2016). Steam-Field Design Overview of The Ulubelu Geothermal Project, Indonesia. *38th New Zealand Geothermal Workshop*, (pp. 1-6). Auckland.

Muffler, P., & Cataldi, R. (1978). Methods for Regional Assessment of Geothermal Resources. *Geothermics, 7*(2-4), 53-89.

Nanlohy, F., Sitorus, K., Kasbani, Dwipa, S., & Simajuntak, J. (2002). Subsurface Geology of the Mataloko Geothermal Field Deduced from MTL-1, MT-1 and MT-2 Wells, Central Flores, East Nusa Tenggara, Indonesia. *Bulletin of the Geological Survey of Japan, 53*(2/3), 329-336.

Nicholson, K. N. (1993). *Geothermal Fluids. Chemistry and Exploration Techniques* (ISBN 3 540 56017 3 ed.). Berlin: Springer Verlag.

Noorollahi, Y. (2005). *Application of GIS and Remote Sensing in Exploration and Environmental Management of Namafjall Geothermal Area, N-Iceland.* Reykjavik: The United Nations University.

Omar, F. (2013). *Directional Well Design, Trajectory and Survey Calculations, with a Case Study in Fiale, Asal Rift, Djibouti.* Reykjavik: United Natios University Geothermal Training Programme (UNU-GTP).

Pradhipta, Y. D., Sutopo, Pratama, H. B., & Adiprana, R. (2019). Natural State Modeling of Mataloko Geothermal Field, Flores Island, East Nusa Tenggara, Indonesia Using TOUGH2 Simulator. *IOP Conference Series: Earth and Environmental Science, 254*, 012027.

Quinlivan, P. (2015). Assessing Geothermal Tariffs in the Face of Uncertainty: A Probabilistic Approach. Melbourne: Prosiding, World Geothermal Congress 2015.

Sitorus, K., Nanlohy, F., & Simanjuntak, J. (2001). Drilling Activity in the Mataloko Geothermal Field, Ngada - NTT, Flores - Indonesia. *Proceedings of the 5th INAGA Annual Scientific Conference & Exhibitions* (pp. 1-6). Yogyakarta: Indonesian Geothermal Association.

Sitorus, K., Sulistyohadi, F., & Simanjuntak, J. (2002). Long Term Flow Test of the MT-2 Well, the Mataloko Geothermal Field, Ngada, Flores Island, Indonesia. *Bulletin of the Geological Survey of Japan, 53*(2/3), 389-397.

Sueyoshi, Y., Matsuda, K., Shimoike, T., Koseki, T., Takahashi, H., Futagoishi, M., . . . Simanjuntak, J. (2002). Exploratory Well Drilling and Discharge Test of Wells MT-1 and MT-2 in the Mataloko Geothermal Field, Flores, Indonesia. *Bulletin of the Geological Survey of Japan, 53*(2/3), 307-321.

Suhanto, E., & Arsadipura, S. (2006). Evaluasi Prospek Lapangan Mataloko dengan Survei Mise-A-La-Masse dan Pengujian Sumur MT-5. *Proceeding Pemaparan Hasil-Hasil Kegiatan Lapangan dan Non Lapangan Tahun 2006* (pp. 1-11). Jakarta: Pusat Sumber Daya Geologi.

Sumotarto, U., Yunis, Y., Hendrasto, F., Pudyastuti, K., Sammuel, E. R., Rizky, D., & Nayoan, A. G. (2021). Geothermal Well Targeting in Consideration To Geological Structures of Mataloko Field, Flores. *IOP Conference Series: Earth and Environmental Science, 819*, 012019.

Suparman. (2009). Sumur Injeksi MT-6 di Lapangan Panas Bumi Mataloko, Kabupaten Ngada, Nusa Tenggara Timur. *Buletin Sumber Daya Geologi, 4*(2), 59-68.

Uchida, T. (2005). Three-Dimensional Magnetotelluric Investigation in Geothermal Fields in Japan and Indonesia. *Proceedings, World Geothermal Congress 2005.* Ankara: International Geothermal Association.

Ulum, B., Nurrohman, Ambarita, E., & Gaos, Y. S. (2017). Energy and Exergy Analysis of Mount Salak Geothermal Power Plant Unit 1-2-3. *International Journal of Technology, 7*, 1217-1228.

UNFCCC/CCNUCC. (2012). *Project Design Document Form for CDM Project Activities*. Washington, D.C.: United Nations.

Usher, G. (2000). Understanding the Resistivities Observed in Geothermal Systems. *Proceedings, World Geothermal Congress 2000.* Kyushu: International Geothermal Association.

Wahdjosoedibjo, A. S., & Hasan, M. (2018). Indonesia's Geothermal Development: Where is it Going? Stanford: Proceedings, 43rd Workshop on Geothermal Reservoir Engineering.

Wahyuningsih, R., & Sitorus, K. (2004). Evaluasi Lapangan Panas Bumi Mataloko Pasca Pengeboran dan Uji Alir Sumur MT-3 dan MT-4. *Proceedings of the 33rd Annual Convention & Exhibition 2004* (pp. 1-13). Bandung: Indonesian Association of Geologist.

Winofa, N. C., Lesmana, A., Pratama, H. B., Saptadji, N. M., & Ashat, A. (2019). The Application of Numerical Simulation Result for Geothermal Financial Model with Probablistic Approach: A Comprehensive Study. *Proceedings, 7th Indonesia International Geothermal Conference & Exhibition (IIGCE) 2019.* Jakarta: Indonesian Geothermal Association.

Yousefi, H., & Ehara, S. (2008). Geothermal Potential Site Selection Using GIS in Iran. *PROCEEDINGS, Thirty-Second Workshop on Geothermal Reservoir Engineering* (pp. 1-9). Stanford: Stanford University.

Zarrouk, S. J., & Moon, H. (2014). Efficiency of Geothermal Power Plants: A Worldwide Review. *Geothermics*, 142-153. doi:10.1016/j.geothermics.2013.11.001

Zeyghami, M. (2010). Thermoeconomic Optimization of Geothermal Flash Steam Power Plants. *Proceedings of the World Geothermal Congress 2010* (pp. 1-8). Denpasar: International Geothermal Association.